Stirling Analysis Comparison of Commercial VS. High-Order Methods

Rodger W. Dyson*, Scott D. Wilson†, Roy C. Tew*, and Rikako Demko†

NASA Glenn Research Center, Cleveland, OH, 44035, USA

Recently, three-dimensional Stirling engine simulations have been accomplished utilizing commercial Computational Fluid Dynamics software. The validations reported can be somewhat inconclusive due to the lack of precise time accurate experimental results from engines, export control/proprietary concerns, and the lack of variation in the methods utilized. The last issue may be addressed by solving the same flow problem with alternate methods. In this work, a comprehensive examination of the methods utilized in the commercial codes is compared with more recently developed high-order methods. Specifically, Lele's Compact scheme and Dyson's Ultra Hi-Fi method will be compared with the SIMPLE and PISO methods currently employed in CFD-ACE, FLUENT, CFX, and STAR-CD (all commercial codes which can in theory solve a three-dimensional Stirling model although sliding interfaces and their moving grids limit the effective time accuracy). We will initially look at one-dimensional flows since the current standard practice is to design and optimize Stirling engines with empirically corrected friction and heat transfer coefficients in an overall one-dimensional model. This comparison provides an idea of the range in which commercial CFD software for modeling Stirling engines may be expected to provide accurate results. In addition, this work provides a framework for improving current one-dimensional analysis codes.

*Aerospace Engineer, Thermal Energy Conversion Branch, Mail Stop 301-2, AIAA Member

†Aerospace Engineer, Sest, Inc.,AIAA Member

Nomenclature

β	Nondimensional Wavenumber
ϵ	Turbulent Dissipation Rate,(m^2/s^3)
η	Kolmogorov Length Scale,(m)
μ	Dynamic (Molecular) Viscosity,$(Ns \cdot m^{-2})$
ν	Kinematic Viscosity,$(\mu \cdot \rho^{-1})$
ρ	Density,$(kg \cdot m^{-3})$
τ_w	Surface Shear Stress,$(kg \cdot m^{-1}s^{-2})$
c	Constant Convective Velocity
$c4o0$	UHF Method - 4 point stencil - no derivatives
$c4o1$	UHF Method - 4 point stencil - one derivative
$c4o2$	UHF Method - 4 point stencil - two derivatives
$c4o3$	UHF Method - 4 point stencil - three derivatives
C_p	Specific Heat Constant Pressure
C_v	Specific Heat Constant Volume
G	Complex Amplification Factor
k	Wavenumber
L	Length of Numerical Domain
r	Courant Number
u_τ	Friction Velocity,$(kg \cdot m^{-3})$
v	Von Neuman Number
CFL	Courant-Friedrichs-Lewy

I. Introduction

Power conversion with free-piston Stirling engines[1] promises to deliver high efficiency, low mass solutions for longer and more varied space missions.[2] In addition to using advanced high-temperature materials to increase the Carnot temperature ratio, it is anticipated that advanced computational fluid dynamics (CFD) will help to identify the following losses[4–6] (also shown in figure 1):

1. Inefficient heat exchange and pressure loss in the heat exchangers (heater,regenerator, and cooler)

2. Gas spring and working space loss due to hysterisis and turbulence,

3. Appendix gap losses due to pumping and shuttle effects,

4. Mixing gas losses from unequal temperature distributions or losses from mixing of gas streams, or elements of gas at different temperatures,

5. Conduction losses from the hot to cold regions

In addition, the following artificial numerical losses must be considered when computational simulations are performed (also shown in figure 1):

1. Moving/deforming mesh losses from repeated low order flow field interpolations,

2. Transient/Unsteady heat transfer and flow loss from inconsistent and inaccurate time discretization,

3. Flow loss from low order approaches resulting in effectively adding artificial dissipation terms along sliding interfaces, at structured/unstructured grid interfaces, and within interior.

Minimizing those artificial losses is best accomplished through higher order approaches.[7] While this approach is common in aeroacoustics, computational electromagnetics, and exterior flow problems, high order techniques have not yet been applied to simulating a Stirling device. Moreover, the following difficulties are often encountered when using high-order approaches:

1. Generation of high-order, smooth, body-fitted grids around complex configurations can be difficult.[8]

2. High-order formulations can lack nonlinear robustness.[8]

3. The general usefulness of high-order methods is limited by first order accurate shock capturing.[9]

Fortunately, with the exception of the possibly random geometry in the regenerator, the free-piston design is essentially smooth and admits curvilinear structured grids (with some geometry simplification). The issue of nonlinear robustness (i.e. maintaining design accuracy with nonlinear equations) is an open issue, but preliminary results are encouraging. And finally, the working gas is subsonic and shockless throughout the entire region[10] (However, steep temperature gradients can exist at solid/fluid interfaces). For these reasons, a high-order approach is investigated for "whole engine" Stirling analysis and compared to commonly used techniques.

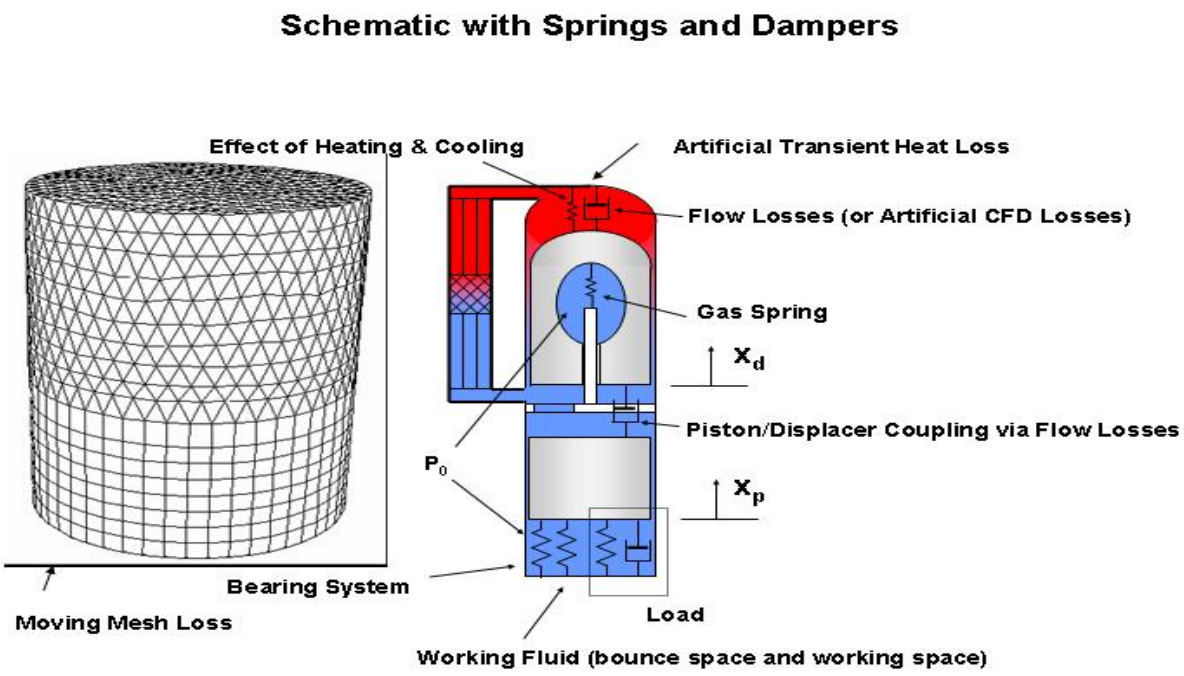

Figure 1. Schematic of Actual and Artificial Numerical Losses in a Free-Piston Convertor

II. Description of the Problem

The dual opposed configuration shown in figure 2 [11,12] is being developed for multimission uses.[13]

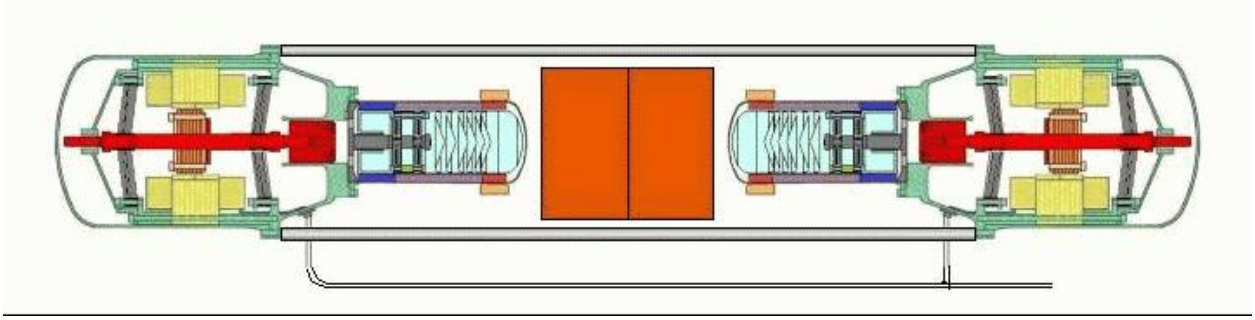

Figure 2. Dual Opposed Stirling Convertors Reduce Vibration

Many methods in general use stop at 4^{th} order accuracy for time dependent problems since they use Runge-Kutta methods. High-order Runge-Kutta methods become notoriously difficult to derive because the number of nonlinear order conditions that need to be solved grows exponentially (i.e., a 12^{th} order method has 7813 nonlinear order conditions). The advantages of using Runge-Kutta methods at orders less than 6 are commonly cited as

flexibility, large stability limits, and ease of programming.[14] The practical limit on their order has been an impediment to the analysis of their use in high order approaches for time dependent applications.[15]

In this paper we use a series of explicit, local, high order methods which have the same order of accuracy in space as in time[16,17] for inviscid flow (lower accuracy in time for viscous flows). These methods use Hermite interpolation on stencils that are four points wide, and a Cauchy-Kowalewski recursive procedure[18] for obtaining time derivatives from the space derivatives of the interpolant. The time derivatives are then used to advance the primitive variables and their spatial derivatives in time with a Taylor series expansion. This general approach is called the Modified Expansion Solution Approximation (MESA) method[19] and the new finite volume variation of this is called the Ultra HI-FI (UHF) method.[20] This method can be used to derive and implement algorithms with arbitrarily high orders of accuracy in multiple space dimensions if their complexity is properly managed and the computer's floating point precision is sufficiently high.[21]

First, some of the known exact solutions of the viscous Burger's equation are provided and the linear case is solved with both state-of-practice Compact schemes, new UHF methods, and various commercial code solvers. The one-dimensional Navier-Stokes equations reduce to the linear viscous Burger's equation in certain circumstances and provide a means for testing both heat transfer effectiveness and turbulent transition efficiency of each method.

III. Exact Solutions For Method Comparison

Since the nonlinear Navier-Stokes equations generally do not have exact solutions nor known stability limits, preliminary development and testing of new numerical methods is best accomplished by starting with the viscous Burger's equation. This equation describes flow behaviour in specialized circumstances, but more importantly, its mathematical properties are very similar to the full Navier-Stokes equations and it admits exact solutions.

For future reference and convenience, some of the known exact solutions are shown below (only the linear viscous Burger's equation will be required in this work).

A. Complete Nonlinear Viscous Burger's Equation

The viscous Burger's equation is written as:

$$\frac{\partial u}{\partial t} + u\frac{\partial u}{\partial x} = \mu\frac{\partial^2 u}{\partial x^2} \tag{1}$$

where u is the convective velocity term and μ can be considered the dynamic viscosity.

Exact steady-state solution, $lim_{t\to\infty}u(x,t)$ exists for the case with boundary conditions:

$$u(0,t) = u_0 \tag{2}$$

$$u(L,t) = 0 \tag{3}$$

and it is given by:

$$u = u_0\bar{u}\left[\frac{1-\exp[\bar{u}Re_L(x/L-1)]}{1+\exp[\bar{u}Re_L(x/L-1)]}\right] \tag{4}$$

where $Re_L = \frac{u_0 L}{\mu}$ (note this is a modified Reynold's number)
$\bar{u}$ is a solution of the equation

$$\frac{\bar{u}-1}{\bar{u}+1} = \exp(-\bar{u}Re_L) \tag{5}$$

Other solutions for the nonlinear viscous burgers equation are:

1.

$$u_t + uu_x - \mu u_{xx} = 0, \mu = 0.1, x \in (0,1) \tag{6}$$

$$u(x,0) = 0, u(1,t) = -tanh\left(\frac{1}{2\mu}\right), u(0,t) = 0 \tag{7}$$

has exact solution

$$u(x,t) = -tanh\left(\frac{x}{2\mu}\right) \tag{8}$$

2. Fully nonlinear equation:

$$u_t + uu_x - \frac{1}{2}(u\dot{u}_x)_x = 0, x \in (0,1) \tag{9}$$

with initial and boundary conditions as:

$$u(x,0) = \exp^x, u(0,t) = 1, u(1,t) = e \tag{10}$$

has the following exact solution $u(x,t) = \exp^x$.

3. An exact solution of the nondimensional form of the Nonlinear Burger's equationn[22]

$$\frac{\partial u}{\partial t} + u\frac{\partial u}{\partial x} = \mu\frac{\partial^2 u}{\partial x^2} \tag{11}$$

Nondimensionalized by:

$$x^* = \frac{x}{L}, u^* = \frac{uL}{\mu}, t* = \frac{\mu}{L^2}t \tag{12}$$

producing:

$$\frac{u^*}{t^*} + u^*\frac{\partial u^*}{\partial x^*} = \frac{\partial^2 u^*}{\partial x^{*2}} \tag{13}$$

One stationary solution is:

$$u^* = -\frac{2\sinh x^*}{\cosh x^* - \exp^{-t^*}} \tag{14}$$

B. Linear Viscous Burger's Equation

For simplicity and more thorough stability analyses, the viscous Burger's equation may be linearized with constant convective velocity, c, and dynamic viscosity, μ:

$$\frac{\partial u}{\partial t} + c\frac{\partial u}{\partial x} = \mu\frac{\partial^2 u}{\partial x^2} \tag{15}$$

The exact steady-state solution with the same boundary conditions as in Eqs.(2) and (3) is:

$$u = u_0\left[\frac{1 - \exp[R_L(x/L - 1)]}{1 - \exp(-R_L)}\right] \tag{16}$$

where $R_L = \frac{cL}{\mu}$ (modified Reynolds number).

The exact solution for the linearized equation with initial condition, $u(x, 0) = sin(kx)$, and periodic boundary conditions is:

$$u(x, t) = \exp(-k^2\mu t)\sin k(x - ct) \tag{17}$$

This is useful for evaluating the temporal accuracy of a method and this will be used in comparing Compact and UHF techniques.[23]

In addition, this equation form also describes the time-accurate temperature distribution in a moving solid or within a moving fluid in a channel in which case $\mu = \alpha = \frac{k}{\rho C_v}$ is interpreted as the thermal diffusivity, and T is the temperature:

$$\frac{\partial T}{\partial t} + u\frac{\partial T}{\partial x} = \alpha\frac{\partial^2 T}{\partial x^2} \tag{18}$$

This will be used for comparing the heat transfer capabilities of Compact, UHF, and commercial code solvers.

C. 2-D Nonlinear Viscous Burgers' Equation

The 2-D Burger's equation with nonlinear convection terms,[24]

$$\frac{\partial u}{\partial t} + u\frac{\partial u}{\partial x} + v\frac{\partial u}{\partial y} - v(\frac{\partial^2 u}{\partial x^2} + \frac{\partial^2 u}{\partial y^2}) - f_x = 0 \tag{19}$$

$$\frac{\partial v}{\partial t} + u\frac{\partial v}{\partial x} + v\frac{\partial v}{\partial y} - v(\frac{\partial^2 v}{\partial x^2} + \frac{\partial^2 v}{\partial y^2}) - f_y = 0 \tag{20}$$

with

$$f_x = -\frac{1}{(1+t)^2} + \frac{x^2+2xy}{(1+t)} + 3x^3y^2 - 2vy \tag{21}$$

$$f_y = -\frac{1}{(1+t)^2} + \frac{y^2+2xy}{(1+t)} + 3y^3x^2 - 2vx \tag{22}$$

has exact solution:

$$u = \frac{1}{1+t} + x^2y \tag{23}$$

$$v = \frac{1}{1+t} + xy^2 \tag{24}$$

D. 2-D Linear Burger's Equation

The 2D (Burger's) linear convection and diffusion equation:[25]

$$u_t + c(u_x + u_y) - \mu(u_{xx} + u_{yy}) = 0, (x,y) \in (-1,1) \times (-1,1); c = 1, \mu = 0.01 \tag{25}$$

with the initial condition $u(x,y,0) = \sin(\pi(x+y))$ and periodic boundary condition has the exact solution is:

$$u(x,y,t) = \exp^{-2\pi\mu t} \sin(\pi(x+y-2ct)) \tag{26}$$

Additional exact solutions may be found in the paper by Benton and Platzman.[26]

IV. Application of Compact Scheme

The currently accepted state-of-the-art approach to high fidelity numerical simulations is based on Lele's 6^{th} order Compact scheme.[27] This approach implicitly solves the spatial derivative terms and utilizes standard Runge-Kutta time advance. Each time step requires solving a tridiagonal matrix given by the equation:

$$\alpha\left(\frac{\partial u}{\partial x}\right)_{i-1}+\left(\frac{\partial u}{\partial x}\right)_{i}+\alpha\left(\frac{\partial u}{\partial x}\right)_{i+1}=a\frac{u_{i+1}-u_{i-1}}{2\Delta x}+b\frac{u_{i+2}-u_{i-2}}{4\Delta x} \tag{27}$$

with $\alpha=1/3, a=14/9, b=1/9$.

Similarly, the second order derivatives are found by:

$$\alpha\left(\frac{\partial^2 u}{\partial x^2}\right)_{i-1}+\left(\frac{\partial^2 u}{\partial x^2}\right)_{i}+\alpha\left(\frac{\partial^2 u}{\partial x^2}\right)_{i+1}=a\frac{u_{i+1}-2u_i+u_{i-1}}{\Delta x^2}+b\frac{u_{i+2}-2u_i+u_{i-2}}{4\Delta x^2} \tag{28}$$

with $\alpha=2/11, a=12/11, b=3/11$.

The 4^{th} order Runge-Kutta method is described by:[24]

$$\begin{aligned}
R(u) &= -cu_x+\mu u_{xx} && (29)\\
u^{(1)} &= u^n+\frac{\Delta t}{2}R^n && (30)\\
u^{(2)} &= u^n+\frac{\Delta t}{2}R^1 && (31)\\
u^{(3)} &= u^n+\Delta t R^2 && (32)\\
u^{n+1} &= u^n+\frac{\Delta t}{6}\left(R^n+2R^{(1)}+2R^{(2)}+R^{(3)}\right) && (33)\\
& && (34)
\end{aligned}$$

with

$$\begin{aligned}
R^{(1)} &= R(u^{(1)})\\
R^{(2)} &= R(u^{(2)})\\
R^{(3)} &= R(u^{(3)})
\end{aligned}$$

The single step 6^{th} order Compact scheme with 4^{th} order Runge-Kutta on a domain $[-4,4]$ is given by:

$$\begin{aligned}
u_i^{n+1} = & && (35)\\
&\left(\tfrac{6296179542799261293r^4}{2934584609881498112}+\tfrac{98816474558753811vr^3}{18549839506204160}-\tfrac{31068146188125r^3}{42158726150464}+\tfrac{55178557611v^2r^2}{19381094656}\right)u_{-4}+\\
&\left(-\tfrac{287760797433vr^2}{133245025760}+\tfrac{324338625r^2}{2422636832}+\tfrac{401096399245v^3r}{583491009024}\right)u_{-4}+\\
&\left(-\tfrac{3588625v^2r}{3898048}+\tfrac{573327vr}{1093840}-\tfrac{75r}{8701}-\tfrac{1230500161v^4}{24196548096}-\tfrac{268897v^3}{1714608}+\tfrac{16675v^2}{127008}-\tfrac{11v}{180}\right)u_{-4}+\\
&\left(-\tfrac{76938698802699r^4}{12527254840352}-\tfrac{6211549394313vr^3}{860382166336}+\tfrac{20491256151r^3}{7918618736}-\tfrac{186196891v^2r^2}{40043584}+\tfrac{1236331119vr^2}{346090976}-\tfrac{1463625r^2}{2502724}\right)u_{-3}+
\end{aligned}$$

$$\left(+\frac{1778984341v^3r}{2210193216}+\frac{77947v^2r}{44296}-\frac{65875vr}{69608}+\frac{75r}{1582}+\frac{454075v^4}{4148928}-\frac{2032591v^3}{24004512}-\frac{1025v^2}{3528}+\frac{25v}{252}\right)u_{-3}+$$
$$\left(\frac{12528089829r^4}{1124897312}+\frac{7466191437vr^3}{646417856}-\frac{22282569r^3}{3652264}+\frac{441v^2r^2}{484}-\frac{18974931vr^2}{2860256}+\frac{103671r^2}{47432}\right)u_{-2}+$$
$$\left(-\frac{111033673v^3r}{66975552}-\frac{49v^2r}{66}+\frac{15479vr}{6328}-\frac{75r}{308}-\frac{2401v^4}{39366}+\frac{267775v^3}{889056}+\frac{49v^2}{162}-\frac{25v}{84}\right)u_{-2}+$$
$$\left(-\frac{211569041160693r^4}{12527254840352}-\frac{7860884553897vr^3}{860382166336}+\frac{85890653865r^3}{7918618736}+\frac{186196891v^2r^2}{40043584}+\frac{2047213695vr^2}{346090976}-\frac{13246263r^2}{2502724}\right)u_{-1}+$$
$$\left(+\frac{3480659477v^3r}{2210193216}-\frac{77947v^2r}{44296}-\frac{198763vr}{69608}+\frac{2637r}{1582}-\frac{454075v^4}{4148928}-\frac{9562127v^3}{24004512}+\frac{1025v^2}{3528}+\frac{221v}{252}\right)u_{-1}+$$
$$\left(\frac{2860573783023483475 5r^4}{1467292304940749056}-\frac{278097527037915r^3}{21079363075232}-\frac{72837778155v^2r^2}{9690547328}+\frac{8619732963r^2}{1211318416}\right)u_0+$$
$$\left(+\frac{19447891v^2r}{5847072}-\frac{50889r}{17402}+\frac{2706289217v^4}{12098274048}-\frac{55091v^2}{63504}+1\right)u_0+$$
$$\left(-\frac{211569041160693r^4}{12527254840352}+\frac{7860884553897vr^3}{860382166336}+\frac{85890653865r^3}{7918618736}+\frac{186196891v^2r^2}{40043584}-\frac{2047213695vr^2}{346090976}-\frac{13246263r^2}{2502724}\right)u_1+$$
$$\left(-\frac{3480659477v^3r}{2210193216}-\frac{77947v^2r}{44296}+\frac{198763vr}{69608}+\frac{2637r}{1582}-\frac{454075v^4}{4148928}+\frac{9562127v^3}{24004512}+\frac{1025v^2}{3528}-\frac{221v}{252}\right)u_1+$$
$$\left(\frac{12528089829r^4}{1124897312}-\frac{7466191437vr^3}{646417856}-\frac{22282569r^3}{3652264}+\frac{441v^2r^2}{484}+\frac{18974931vr^2}{2860256}+\frac{103671r^2}{47432}\right)u_2+$$
$$\left(+\frac{111033673v^3r}{66975552}-\frac{49v^2r}{66}-\frac{15479vr}{6328}-\frac{75r}{308}-\frac{2401v^4}{39366}-\frac{267775v^3}{889056}+\frac{49v^2}{162}+\frac{25v}{84}\right)u_2+$$
$$\left(-\frac{76938698802699r^4}{12527254840352}+\frac{6211549394313vr^3}{860382166336}+\frac{20491256151r^3}{7918618736}-\frac{186196891v^2r^2}{40043584}-\frac{1236331119vr^2}{346090976}-\frac{1463625r^2}{2502724}\right)u_3+$$
$$\left(-\frac{1778984341v^3r}{2210193216}+\frac{77947v^2r}{44296}+\frac{65875vr}{69608}+\frac{75r}{1582}+\frac{454075v^4}{4148928}+\frac{2032591v^3}{24004512}-\frac{1025v^2}{3528}-\frac{25v}{252}\right)u_3+$$
$$\left(\frac{6296179542799261293r^4}{2934584609881498112}-\frac{98816474558753811vr^3}{18549839506204160}-\frac{31068146188125r^3}{42158726150464}+\right.$$
$$\left.\frac{55178557611v^2r^2}{19381094656}+\frac{287760797433vr^2}{133245025760}+\frac{324338625r^2}{2422636832}\right)u_4+$$
$$\left(-\frac{401096399245v^3r}{583491009024}-\frac{3588625v^2r}{3898048}-\frac{573327vr}{1093840}-\frac{75r}{8701}-\frac{1230500161v^4}{24196548096}+\frac{268897v^3}{1714608}+\frac{16675v^2}{127008}+\frac{11v}{180}\right)u_4$$

The linearized viscous Burger's equation (Eq. 15) is solved with this Compact scheme with multiple domain sizes to demonstrate the dependence of the implicitly derived spatial derivatives (and the stability limit) on the size of the domain. A Fourier stability analysis is performed and the stability of the Compact scheme as a function of Courant ($r=\frac{c\Delta t}{\Delta x}$), Von Neumann ($v=\frac{\mu\Delta t}{\Delta x^2}$) numbers, and $\beta=\Delta xk$ is derived as:

$$\Re(G)= \tag{36}$$
$$\frac{2860573783023483475 5r^4}{1467292304940749056}-\frac{278097527037915r^3}{21079363075232}-\frac{72837778155v^2r^2}{9690547328}+\frac{8619732963r^2}{1211318416}$$
$$+\frac{19447891v^2r}{5847072}-\frac{50889r}{17402}+\frac{2706289217v^4}{12098274048}-\frac{55091v^2}{63504}+$$
$$\left(-\frac{211569041160693r^4}{6263627420176}+\frac{85890653865r^3}{3959309368}+\frac{186196891v^2r^2}{20021792}-\frac{13246263r^2}{1251362}\right)\cos(\beta)+$$
$$\left(-\frac{77947v^2r}{22148}+\frac{2637r}{791}-\frac{454075v^4}{2074464}+\frac{1025v^2}{1764}\right)\cos(\beta)+$$
$$\left(\frac{12528089829r^4}{562448656}-\frac{22282569r^3}{1826132}+\frac{441v^2r^2}{242}+\frac{103671r^2}{23716}\right)\cos(2\beta)+$$
$$\left(-\frac{49v^2r}{33}-\frac{75r}{154}-\frac{2401v^4}{19683}+\frac{49v^2}{81}\right)\cos(2\beta)+$$
$$\left(-\frac{76938698802699r^4}{6263627420176}+\frac{20491256151r^3}{3959309368}-\frac{186196891v^2r^2}{20021792}-\frac{1463625r^2}{1251362}\right)\cos(3\beta)+$$

$$\left(+\frac{77947v^2r}{22148}+\frac{75r}{791}+\frac{454075v^4}{2074464}-\frac{1025v^2}{1764}\right)\cos(3\beta)+$$
$$\left(\frac{6296179542799261293r^4}{1467292304940749056}-\frac{31068146188125r^3}{21079363075232}+\frac{55178557611v^2r^2}{9690547328}+\frac{324338625r^2}{1211318416}\right)\cos(4\beta)$$
$$\left(-\frac{3588625v^2r}{1949024}-\frac{150r}{8701}-\frac{1230500161v^4}{12098274048}+\frac{16675v^2}{63504}\right)\cos(4\beta)+1$$

The imaginary part of the amplification factor is:

$$\begin{aligned}\Im(G)=&\\ &\left(\frac{7860884553897vr^3}{430191083168}-\frac{2047213695vr^2}{173045488}-\frac{3480659477v^3r}{1105096608}+\frac{198763vr}{34804}+\frac{9562127v^3}{12002256}-\frac{221v}{126}\right)\sin(\beta)\\ &+\left(-\frac{7466191437vr^3}{323208928}+\frac{18974931vr^2}{1430128}+\frac{111033673v^3r}{33487776}-\frac{15479vr}{3164}-\frac{267775v^3}{444528}+\frac{25v}{42}\right)\sin(2\beta)\\ &+\left(\frac{6211549394313vr^3}{430191083168}-\frac{1236331119vr^2}{173045488}-\frac{1778984341v^3r}{1105096608}+\frac{65875vr}{34804}+\frac{2032591v^3}{12002256}-\frac{25v}{126}\right)\sin(3\beta)\\ &+\left(-\frac{9881647455875381 1vr^3}{9274919753102080}+\frac{287760797433vr^2}{66622512880}-\frac{401096399245v^3r}{291745504512}-\frac{573327vr}{546920}+\frac{268897v^3}{857304}+\frac{11v}{90}\right)\sin(4\beta)\end{aligned} \tag{37}$$

The amplification factor is simply, $|G|=\sqrt{\Re(G)^2+\Im(G)^2}$, and the range of stability (green area) is shown in Fig. 3. Notice how the stable region changes as the domain size, maxi (the number of grid points in each direction), changes. Explicit spatial derivative operators do not exhibit this behavior since the stencil size remains constant regardless of domain size.

V. Application of UHF Method

The MESA and Ultra Hi-Fi Methods are actually a procedure for designing ever more accurate numerical methods in which additional information is stored at each cell or grid point. For this comparison, the solution variable and up to it's third spatial derivative will be stored at each grid. The notation, *c4od*, represents an UHF method with a 4 point stencil and only the solution variable and up to d derivatives on the grid. The basic procedure has been previously published for inviscid problems.[20]

The c4o0 UHF method will use a 4 point interpolation stencil to determine spatial derivatives as shown in Fig 4. A simple 1^{st} order Taylor series in time is used:

$$u_i^{n+1}=u^n+u_t(\Delta t) \tag{38}$$

in which the time derivative is found from the governing equation (Eq. 15) to be:

$$\frac{\partial u}{\partial t}=-cu_x+\mu u_{xx} \tag{39}$$

and the solution variables, u, u_x, u_{xx}, are interpolated to the center of the four-point

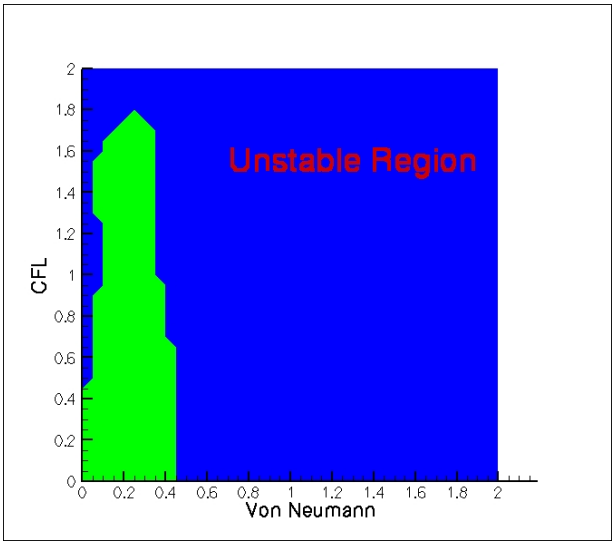

(a) MAXI=2

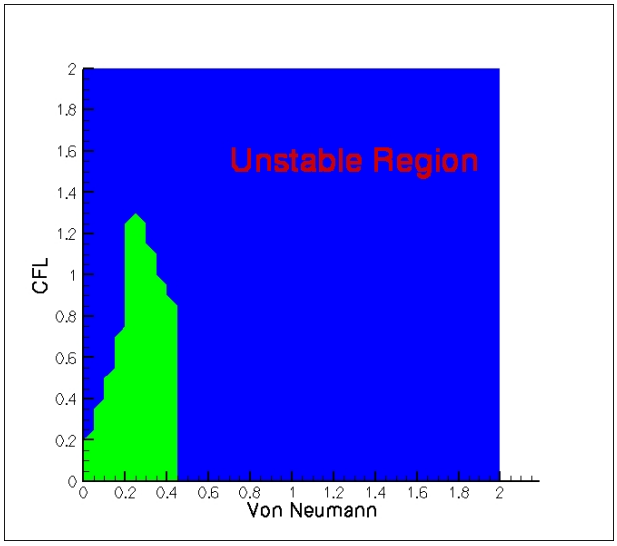

(b) MAXI=3

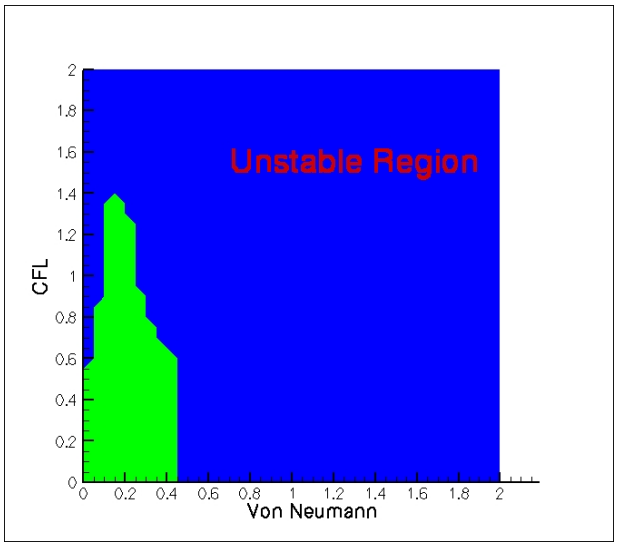

(c) MAXI=4

Figure 3. Lele Compact Linear Viscous Burgers Equation Stability Range

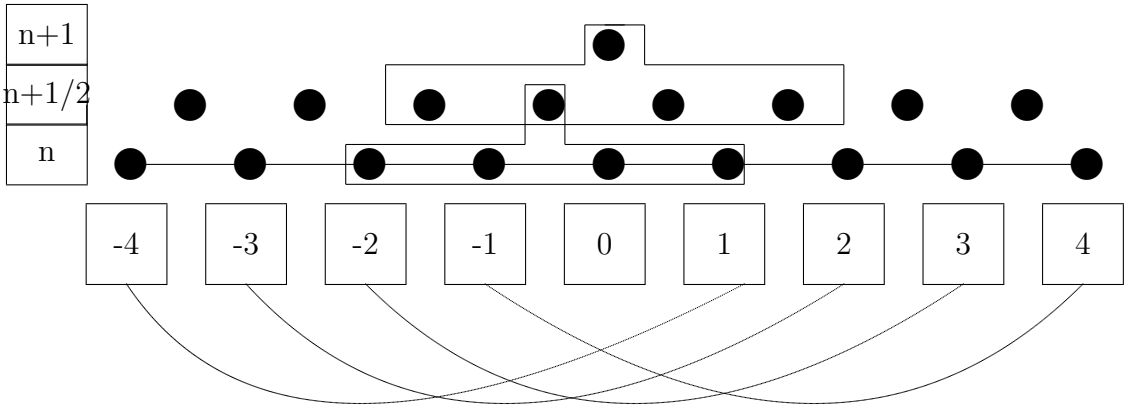

Figure 4. UHF Staggered Grid Diagram

stencil using:

$$u_i^n = \frac{1}{16}\left(-u_{i-\frac{3}{2}} + 9u_{i-\frac{1}{2}} + 9u_{i+\frac{1}{2}} - u_{i+\frac{3}{2}}\right) \tag{40}$$

$$u_{x_i}^n = -\frac{-u_{i-\frac{3}{2}} + 27u_{i-\frac{1}{2}}) - 27u_{i+\frac{1}{2}} + u_{i+\frac{3}{2}}}{24\Delta x} \tag{41}$$

$$u_{xx_i}^n = -\frac{-u_{i-\frac{3}{2}} + u_{i-\frac{1}{2}} + u_{i+\frac{1}{2}} - u_{i+\frac{3}{2}}}{2\Delta x^2} \tag{42}$$

This results in a single time equation:

$$\begin{aligned} u_i^{n+(1/2)} = &\left(\frac{\mu\Delta t}{2h^2} - \frac{c\Delta t}{24h} - \frac{1}{16}\right) uu_{i-\frac{3}{2}} + \left(-\frac{\mu\Delta t}{2h^2} + \frac{9c\Delta t}{8h} + \frac{9}{16}\right) uu_{i-\frac{1}{2}} + \\ &\left(-\frac{\mu\Delta t}{2h^2} - \frac{9c\Delta t}{8h} + \frac{9}{16}\right) uu_{i+\frac{1}{2}} + \left(\frac{\mu\Delta t}{2h^2} + \frac{c\Delta t}{24h} - \frac{1}{16}\right) uu_{i+\frac{3}{2}} \end{aligned} \tag{43}$$

And after two time steps, the original "unstaggered" grid has been updated with the following:

$$\begin{aligned} u_i^{n+1} = \; & u_{i-3}\left(\frac{\mu\Delta t}{2h^2} - \frac{c\Delta t}{24h} - \frac{1}{16}\right)^2 + \\ & 2\left(-\frac{\mu\Delta t}{2h^2} + \frac{9c\Delta t}{8h} + \frac{9}{16}\right) u_{i-2}\left(\frac{\mu\Delta t}{2h^2} - \frac{c\Delta t}{24h} - \frac{1}{16}\right) + \\ & \left(\left(-\frac{\mu\Delta t}{2h^2} + \frac{9c\Delta t}{8h} + \frac{9}{16}\right)^2 + 2\left(-\frac{\mu\Delta t}{2h^2} - \frac{9c\Delta t}{8h} + \frac{9}{16}\right)\left(\frac{\mu\Delta t}{2h^2} - \frac{c\Delta t}{24h} - \frac{1}{16}\right)\right) u_{i-1} + \\ & \left(2\left(-\frac{\mu\Delta t}{2h^2} - \frac{9c\Delta t}{8h} + \frac{9}{16}\right)\left(-\frac{\mu\Delta t}{2h^2} + \frac{9c\Delta t}{8h} + \frac{9}{16}\right) + \right. \\ & \left. 2\left(\frac{\mu\Delta t}{2h^2} - \frac{c\Delta t}{24h} - \frac{1}{16}\right)\left(\frac{\mu\Delta t}{2h^2} + \frac{c\Delta t}{24h} - \frac{1}{16}\right)\right) u_i + \end{aligned}$$

$$\left(\left(-\frac{\mu\Delta t}{2h^2}-\frac{9c\Delta t}{8h}+\frac{9}{16}\right)^2+2\left(-\frac{\mu\Delta t}{2h^2}+\frac{9c\Delta t}{8h}+\frac{9}{16}\right)\left(\frac{\mu\Delta t}{2h^2}+\frac{c\Delta t}{24h}-\frac{1}{16}\right)\right)u_{i+1}+$$
$$2\left(-\frac{\mu\Delta t}{2h^2}-\frac{9c\Delta t}{8h}+\frac{9}{16}\right)\left(\frac{\mu\Delta t}{2h^2}+\frac{c\Delta t}{24h}-\frac{1}{16}\right)u_{i+2}$$
$$+\left(\frac{\mu\Delta t}{2h^2}+\frac{c\Delta t}{24h}-\frac{1}{16}\right)^2u_{i+3} \tag{44}$$

As was done with the Compact algorithm, a Fourier stability analysis is completed with the real part of amplification factor:

$$\begin{aligned}\Re(G) &= (1152)^{-1}(-2920v^2+288r(4r-5)+9\left(348v^2+16(1-4r)r+63\right)\cos(\beta) \\ &\quad -18\left(12v^2+16r(4r-5)+9\right)\cos(2\beta)+\left(9(1-8r)^2+4v^2\right)\cos(3\beta)+738)\end{aligned} \tag{45}$$

And the imaginary part of the amplification factor:

$$\Im(G)=\frac{1}{48}v(-8r+(8r-1)\cos(\beta)+5)(\sin(2\beta)-26\sin(\beta)) \tag{46}$$

The amplification factor, $|G|=\sqrt{\Re(G)^2+\Im(G)^2}$, is plotted as in Fig. 5 as a function of Courant and Von Neumann numbers, and $\beta=\Delta xk$. The left figure (a) unwraps the polar plot in right figure (b). As β increases the amplification factor simply repeats. It has been traditional to use a polar plot due to this property. However, as soon as derivative information is stored on the grid, the amplification factor continues to vary as $\beta>2\pi$. This is due to the ability of these techniques to carry ultra-short wave information. Amplification factors larger than one for any wavenumber imply it is an unstable method.

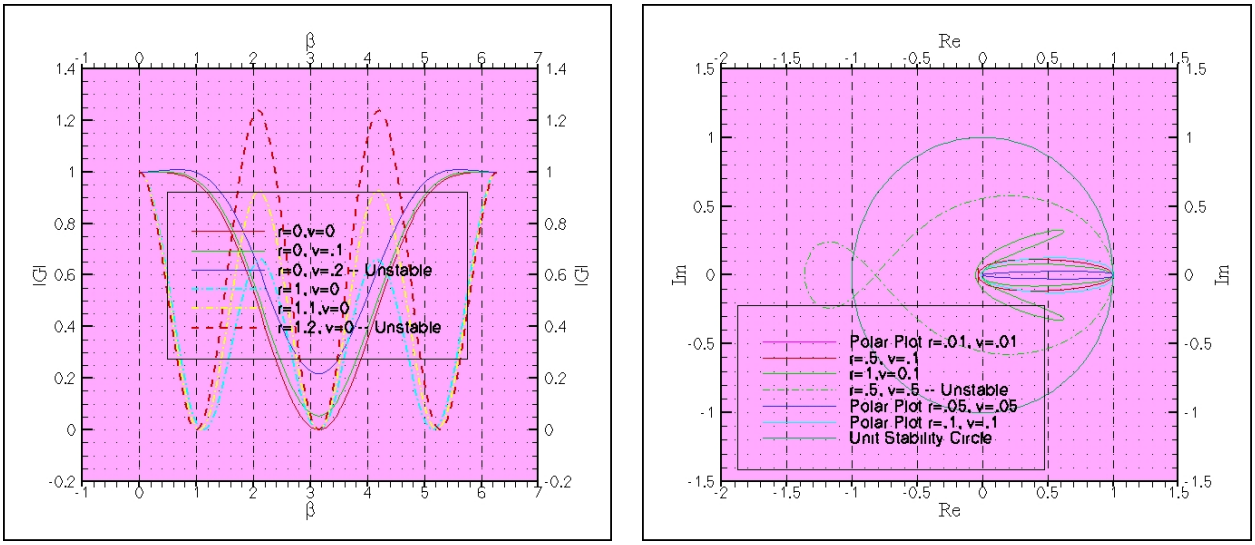

(a) Amplification - c4o0

(b) Polar Diagram

Figure 5. c4o0 - Linear Viscous Burgers Equation

Following this same procedure, but adding additional derivatives on the grid to produce methods, $c4o1$, $c4o2$, and $c4o3$ results in the algorithms shown in the appendix.

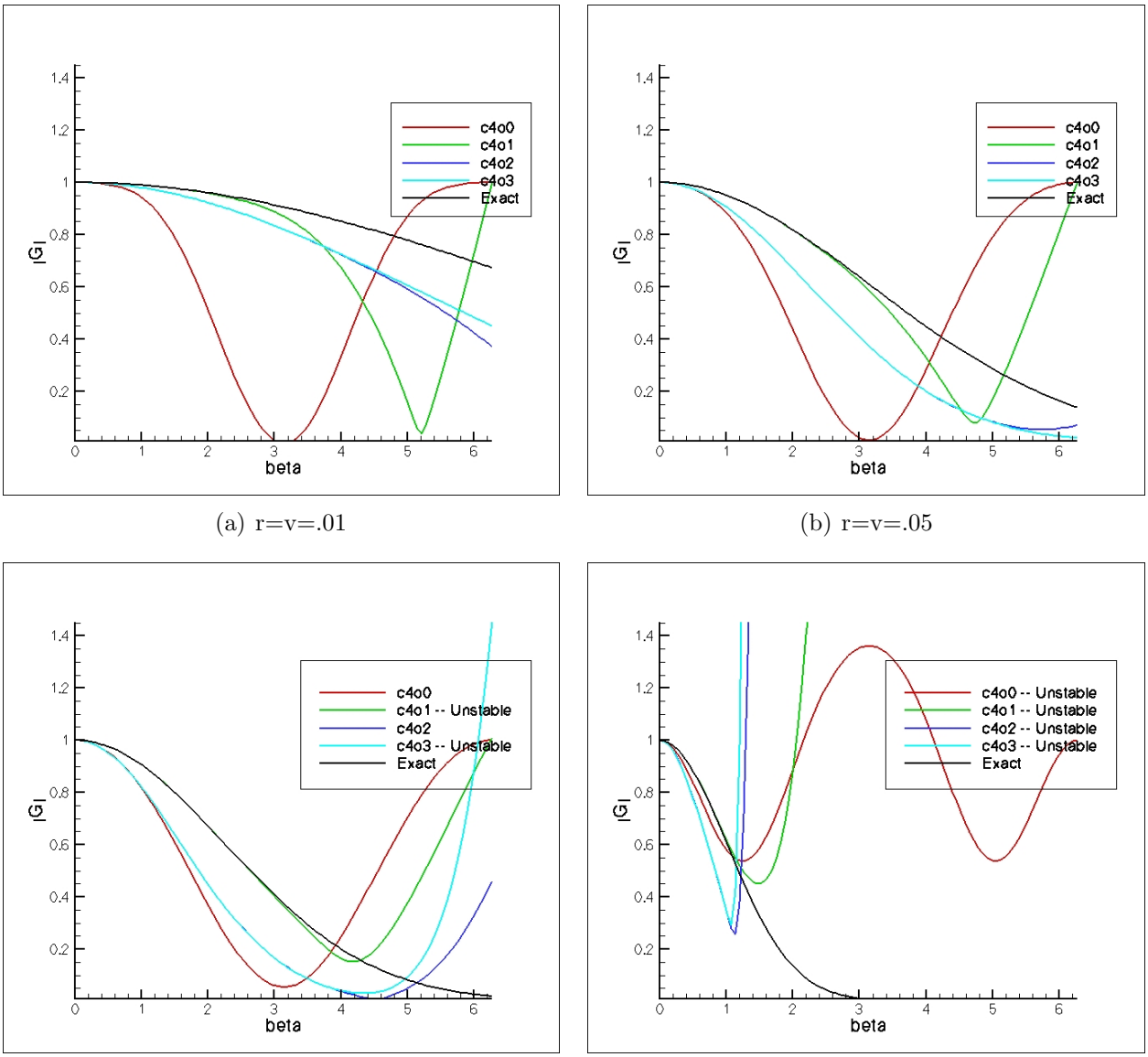

(a) r=v=.01

(b) r=v=.05

(c) r=v=.10

(d) r=v=.5

Figure 6. Ampification/Stability Factor Comparison

The full equations shown in the appendix are required to perform the Fourier stability analysis to enable true method comparisons. The exact amplification factor is also shown since we know the exact solution. Notice in Fig. 6 that the various UHF methods more closely approach the exact ampification factor as the number of solution derivatives on the grid increases. Since the UHF methods can resolve ultra-short waves, the wavenumber range in the figure could be extended past $k = 2\pi$.

The stability region for all the UHF methods is shown in Fig. 7. This gives an indication

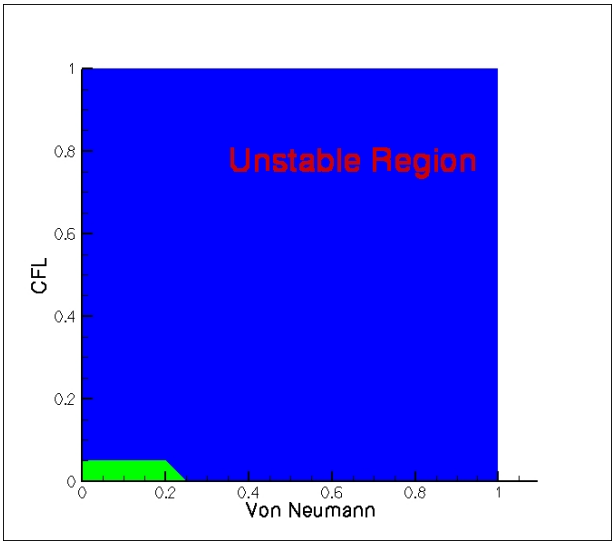

(a) c4o1

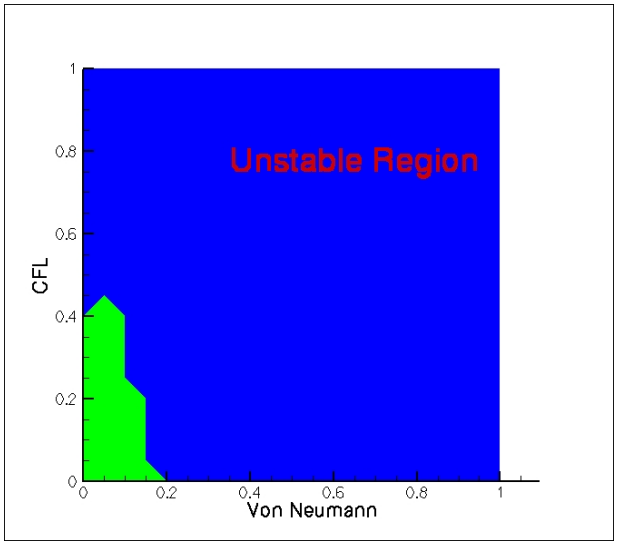

(b) c4o2

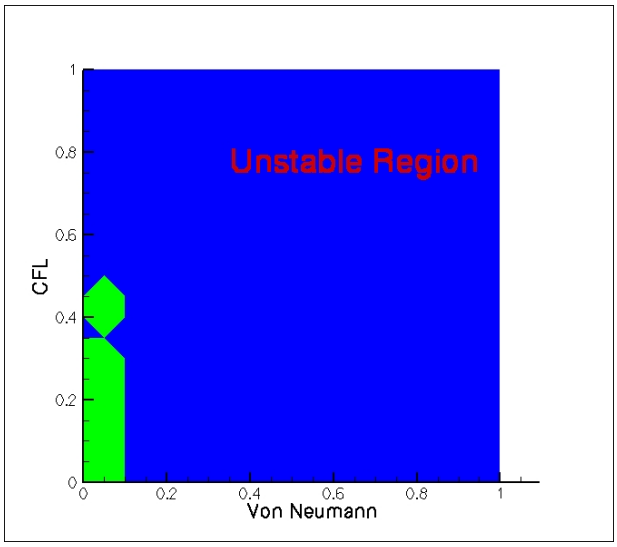

(c) c4o3

Figure 7. UHF Linear Viscous Burgers Equation Stability Range

of the allowable time step as the dynamic viscosity and convective terms vary. Notice (see definition of Von Neuman number given earlier) the role viscosity plays in reducing time step size. Fortunately, the viscosity, μ is a small term generally compared to convection, c. The Compact scheme has larger allowable time steps as shown in Fig. 3 for a given grid. However, more grid is required for the Compact scheme as shown in the next section and despite this apparent advantage, a coarser grid actually results in an effectively larger time step for the UHF methods.

VI. Application of the SIMPLE/PISO Methods

The Semi-Implicit Method for Pressure-Linked Equations (SIMPLE) method[28] and Pressure Implicit with Splitting of Operators (PISO) method[29,30] are the mainstay of commercial fluid dynamics solvers.

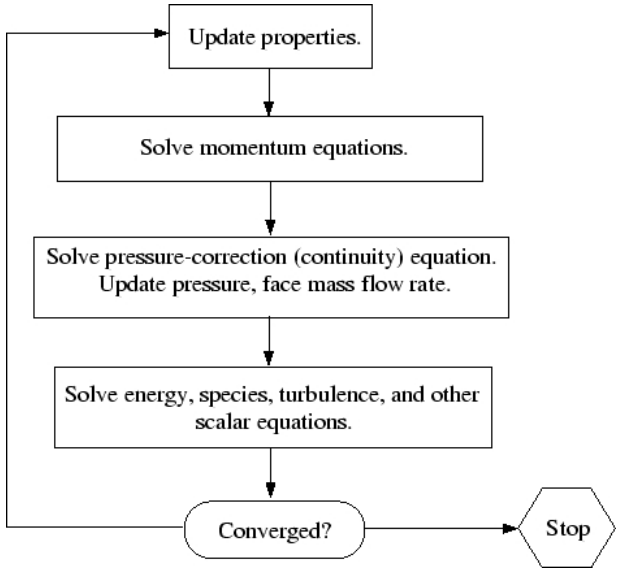

(a) Segregated Process

Figure 8. Overview of Segregated Solution Technique

An overview of the SIMPLE method is:

- Start the iterative process by guessing the pressure field.
- Use those pressure values to determine the velocity from the momentum equations.
- Determine a pressure correction such that the continuity equation is satisfied.
- Find corresponding velocity corrections, and use new pressure and velocity.
- Repeat this until a velocity field is found that does satisfy continuity.

The governing equations are linearized to produce a system of linear equations with one equation for each cell in the domain. A point implicit (Gauss-Seidel) linear equation solver is used in conjunction with an algebraic multigrid method to solve the resultant scalar system of equations.

The time stepping is first order accurate implicit, and the spatial accuracy is second order.

The PISO algorithm moves the repeated calculations required by SIMPLE inside the solution stage of the pressure-correction equation to more closely satisfy the continuity and momentum equations. The PISO method takes more time per iteration, but often requires fewer iterations, particularly for transient problems as will be demonstrated next.

Finally, the stability limits of these two approaches are large (limited by the need for accuracy) compared to the Compact and UHF methods due to implicit time-stepping.

VII. Nonlinear Navier Stokes – 1D

We will now test these techniques on an example of the one-dimensional Navier-Stokes equations that reduces to a one-dimensional heat transfer problem governed by the linear viscous Burger's equation. This is what is solved in Sage/GLIMPS[32] and HFAST[33] to produce reasonable one-dimensional Stirling analysis solutions in industry.

The one-dimensional Navier-Stokes equations can be written as:[23]

$$\frac{\partial U}{\partial t} + \frac{\partial E}{\partial x} = \frac{\partial E_v}{\partial x} \tag{47}$$

$$U = \begin{pmatrix} \rho \\ \rho u \\ E_t \end{pmatrix} E = \begin{pmatrix} \rho u \\ \rho u^2 + p \\ (E_t + p)u \end{pmatrix} E_v = \begin{pmatrix} 0 \\ \tau_{xx} \\ -u\tau_{xx} + q_x \end{pmatrix} \tag{48}$$

$$E_t = \rho\left(e + \frac{u^2}{2}\right) \quad \tau_{xx} = \frac{4}{3}\mu u_x \quad q_x = -k\frac{\partial T}{\partial x} \quad T = \frac{p}{\rho R} \quad k = \frac{\mu c_p}{Pr} \tag{49}$$

Sage/Glimps[32] utilize a slightly different form:

$$\frac{\partial U}{\partial t} + \frac{\partial E}{\partial x} = \frac{\partial E_v}{\partial x} + Q \tag{50}$$

$$U = \begin{pmatrix} \rho \\ \rho u \\ E_t \end{pmatrix} E = \begin{pmatrix} \rho u \\ \rho u^2 + p \\ (E_t + p)u \end{pmatrix} E_v = \begin{pmatrix} 0 \\ 0 \\ q_i \end{pmatrix} Q = \begin{pmatrix} 0 \\ C_f \rho u \\ Q_5 \end{pmatrix} \tag{51}$$

$$E_t = \rho\left(e + \frac{u^2}{2}\right) \quad \tau_{xx} = \frac{4}{3}\mu u_x \quad q_i = -<k>\frac{\partial T}{\partial x}\frac{\rho|u|}{<\rho|u|>} \quad T = \frac{p}{\rho R} \quad k = \frac{\mu c_p}{Pr} \tag{52}$$

Notice that Stoke's stress tensor is replaced by source terms. This also simplifies the numerics since only a single second derivative, $\frac{\partial q_i}{\partial x}$, must be calculated compared to three in Eq. 47. We will utilize the standard Navier-Stokes form for comparison with commercial software. Extension of these ideas to the GLIMPS form is direct.

A. Convection and Diffusion

Few exact solutions exist for the Navier-Stokes equations and therefore validating commercial codes is typically done with only approximate experimental information. One special case that both has an exact solution and yet includes heat transfer physics relevant to oscillating Stirling engines will be shown.

First, commercial codes operate either in two or three dimensions. However, it is possible to cajole the commercial code into solving a one-dimensional problem by solving the full Navier-Stokes equations with an inherently one-dimensional problem such as flow through a pipe with an initial temperature "shock" as shown in Fig. 9.

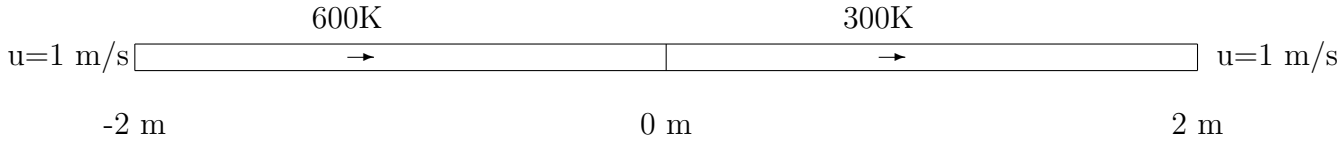

Figure 9. Heat Transfer Test

This problem can be solved with either two or three-dimensional solvers and it reduces to the one-dimensional Navier-Stokes Eq. 47. Since the density and velocity are constant, both the continuity and momentum equations are satisfied. Only the energy equation actually needs to be solved:

$$\frac{\partial E_t}{\partial t} + \frac{\partial}{\partial x}\left((\rho C_v T + p)u - \frac{4}{3}\mu u u_x + q_x\right) = 0 \tag{53}$$

Using, $E_t = \rho C_v T$, and dropping out terms that are zero, we have the following reduced form of the energy equation:

$$\rho C_v \frac{\partial T}{\partial t} = \rho C_v u \frac{\partial T}{\partial x} = k\frac{\partial^2 T}{\partial x^2} \tag{54}$$

Finally, dividing by ρC_v and for essentially incompressible flows replacing C_v with C_p, we have the following transport (linear viscous Burger's equation):

$$\frac{\partial T}{\partial t} + u\frac{\partial T}{\partial x} = \alpha\frac{\partial^2 T}{\partial x^2} \tag{55}$$

with the thermal diffusivity $\alpha = \frac{k}{\rho C_p}$.

Furthermore, commercial solvers utilize the dimensional form of the Navier-Stokes, but by utlizing the following non-dimensionalization ($*$ = nondimensional quantity):

$$T^* = \frac{T}{T_0}, \quad x^* = \frac{x}{L}, \quad t^* = \frac{t}{\tau_0}, u^* = u\frac{\tau_0}{L}, \quad \alpha^* = \frac{\tau_0}{L^2}\alpha \tag{56}$$

and using the following nondimensional boundary conditions:

$$\begin{aligned} &T^*(x*, 0) = 2 \; or \; 1, \quad x \in [-2, 2], \quad t^* = [0, 1], \\ &u^* = 1.0, \Delta x^* = .1, \Delta t^* = .01, \alpha^* = .03003 \end{aligned} \tag{57}$$

We have an exact solution, by the separation-of-variables,[34] (as N is large):

$$T^*(x^*,t^*) = 1 + 0.5 - \frac{2}{\pi}\sum_{k=1}^{N} \sin\left[(2k-1)\frac{\pi(x^* - u^*t^*)}{L}\right] \frac{\exp[-\alpha^*(2k-1)^2\pi^2 t^*/L^2]}{2k-1} \tag{58}$$

And finally, by choosing the characteristic constants as:

$$\tau_0 = 1s, \quad L = 1m, \quad T_0 = 300K \tag{59}$$

We have the following problem definition for the commercial solvers:

$$\begin{aligned} &x \in [-2m, 2m], \quad T \in [300K, 600K], \quad t \in [0s, 1s], \quad u = 1m/s, \\ &\Delta x = .1m, \quad \Delta t = .01s, \quad \alpha = .03003m^2/s, \quad \rho = 998.2kg/m^2, \\ &C_p = 4182J/(kg \cdot K), \quad k = 125359J/(s \cdot K), \quad p = 101325 \ \ Pa \end{aligned} \tag{60}$$

This problem is solved and the results are compared as various techniques are applied to the problem. In Fig. 10, the exact solution is shown along with four UHF techniques, a 6^{th} order Compact scheme, a segregated spatially and temporally implicit method (SIMPLE) used in Fluent, a coupled spatially and temporally implicit method (PISO) used in Fluent, and a segregated central difference with a blended (averaged) Euler and Crank-Nicolson technique used in CFD-ACE. Fluent only allows 1^{st} order accuracy in time when moving meshes are applied as when the Stirling engine is simulated. However, CFD-ACE allows for up to 2^{nd} order accuracy in time when the meshes are compressed with a spring analogy.

The best techniques in this test case are the Compact and c4o3 UHF schemes. The commercially used solvers are noticeably less able to model time accurate heat transfer. However, the coupled solver should be used when commercial codes are applied to oscillating Stirling simulations and when available, 2^{nd} order time accuracy should be used (as when using CFD-ACE).

VIII. Fidelity and Turbulence Transition

Modeling turbulence transition is a difficult problem due to the large disparity in both spatial and temporal scales caused when velocity gradients are high. In the Stirling engine velocity gradients are high near walls and regions of sheared flow due to oscillating/reversing flows. As the velocity gradients increase, the flow becomes rotational, leading to a vigorous stretching of vortex lines, which cannot be supported in two dimensions.[24] For this reason, truly turbulent simulations cannot be done in one-dimension.

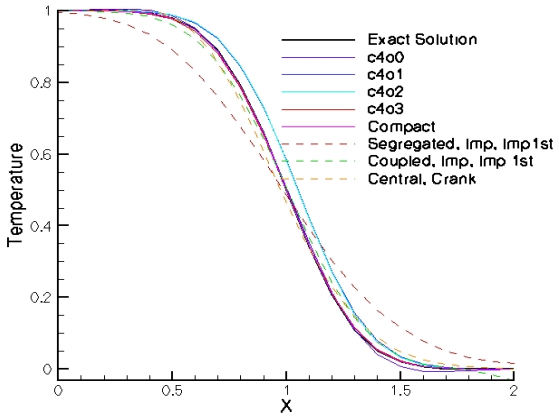

(a) Bird's View

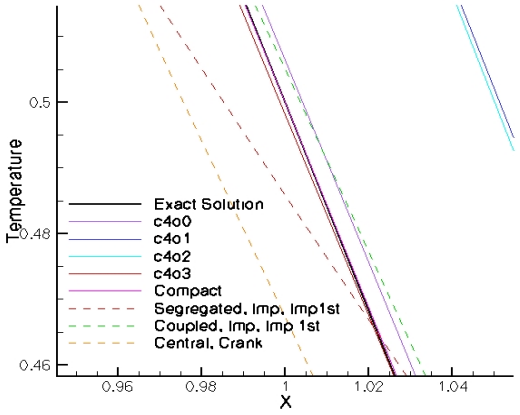

(b) Temperature Slope

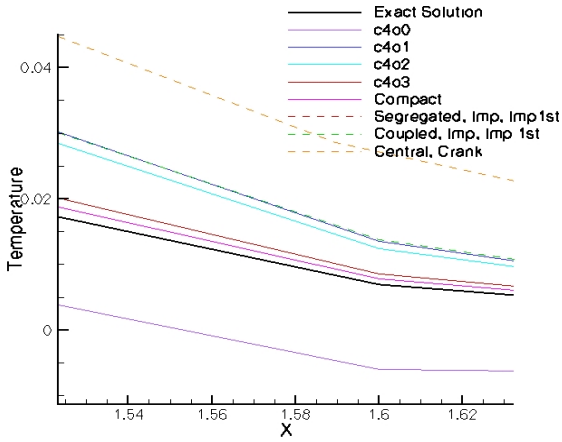

(c) Close-Up

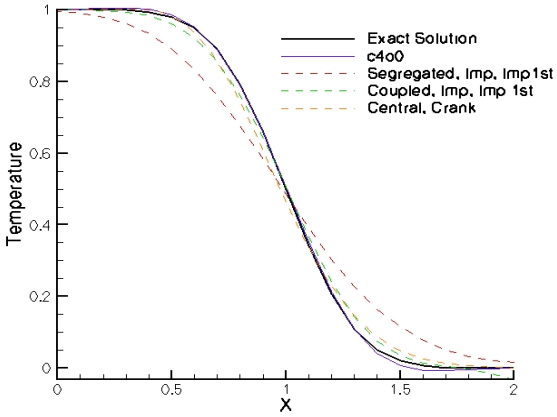

(d) Commercial Comparison

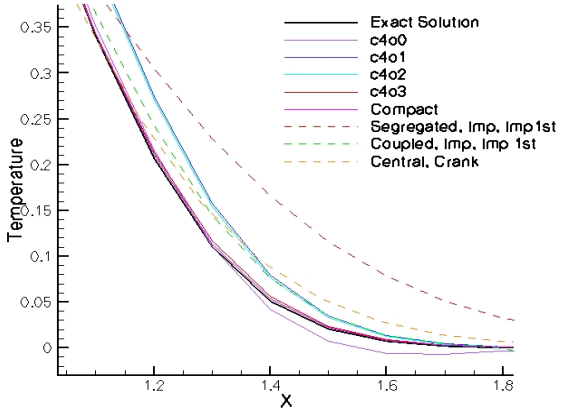

(e) Lower Curve

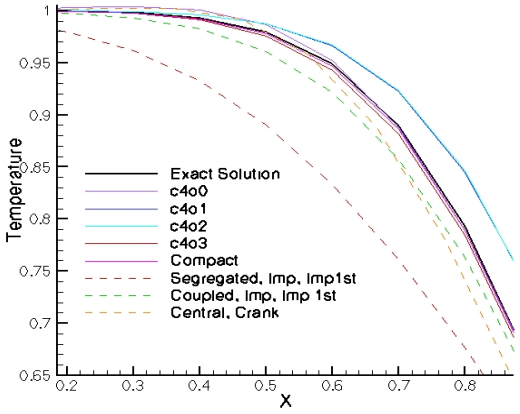

(f) Upper Curve

Figure 10. Heat Diffusion and Convection Comparison

The Stirling engine exhibits turbulent and laminar behaviour simultaneously.[35] It is desirable therefore to avoid a Reynolds Averaged approach since the time averaged equations combined with some turbulence model[36–38] assumes turbulence everywhere. One promising approach is Large Eddy Simulation (LES) in which the Navier-Stokes equations are solved in time, but with spatial filtering applied, leaving the small eddies still unresolved. Since small eddies are essentially isotropic, the modeling is much easier compared to Reynolds time averaging. Moreover, the entire flow is bounded by walls making boundary condition specification much easier than the typical open domain problems encountered in modeling, for example, jet flow turbulence.

The smallest scales of turbulence are the Kolmogorov scales of length, time and velocity:[39]

$$\eta = (\nu^3/\epsilon)^{1/4}, \quad \tau = (\nu/\epsilon)^{1/2}, \quad v = (\nu\epsilon)^{1/4} \tag{61}$$

where ν is the kinematic viscosity, and ϵ is the dissipation rate. The Reynolds number in the Kolmogorov region, $Re = v\eta/\nu = 1$, shows the ratio of inertial and visous forces is unity because most of the energy is dissipated in this wavenumber region.

In small Stirling engines we can estime the smallest scales as follows. With the average flow assumptions for Helium in the engine:

$$\begin{gathered}\mu = 350e-7(Ns/m^2), \quad \nu = 502e-6(m^2/s), \quad k = 278e-3W/(mK), \\ \alpha = 29.9341e-6m^2/s, \quad Pr = 0.654, \quad \omega = 2\pi f = 502.655(rad/s), \\ C_p = 5.19e3J/(kgK), T = 700K, \quad p = 2.6e6Pa, \quad \rho = 1.78838(kg/m^3)\end{gathered} \tag{62}$$

Then from West,[40] for oscillating flow, the average thermal boundary layer thickness, $\sqrt{2\alpha/\omega} = .345115mm$, and the average flow boundary layer thickness, $\sqrt{2\nu/\omega} = 1.41329mm$.

The maximum surface shear stress may be approximated with this information by (assuming average maximum flow speed of $10m/s$ and using the flow boundary layer thickness):

$$\tau_w = \mu\frac{\Delta u}{\Delta y} = .247649N/m^2 \tag{63}$$

The friction velocity, $u_\tau = \sqrt{\frac{\tau_w}{\rho}} = .372125m/s$, is then used in the following equation for dissipation in channel flow:[39]

$$\epsilon \approx 2u_\tau^2 U_m/.0253007m) = 54.7325m^2/s^3 \tag{64}$$

Finally, we can estimate the Kolmogorv spatial wave length as:

$$\eta = (\nu^3/\epsilon)^{1/4} = 1.23301mm \tag{65}$$

Assuming a representative engine length of ($1in. = 25.3007mm$), the domain consists of 20 to 30 Kolmogorov wavelengths, or roughly 8000 regions (Kolmogorov boxes) in 3D where isotropic turbulence modeling can be employed. This corresponds to a turbulent Reynolds number of $Re_\tau = u_\tau(.0253007m)/(2\nu) = 9.37751$. This is low Reynolds number flow and appears ideal for applying Large Eddy Simulation.

One would like to model the smallest turbulent scales, which in the case of LES is the Kolmogorov wavenumber range. The allowable time should also be of the same order as the Kolmogorov time scale.

$$\tau = (\nu/\epsilon)^{1/2} = .00302s \tag{66}$$

This time scale is not prohibitive, since the time step size is already smaller than this in current commercial simulations due to the numerical issues involving moving grids.

We would like to utilize the most efficient technique to minimize the computational cost. We know the minimum wavelengths required to simulate turbulence in the Stirling engine and the wave convection/dissipation problem solution from Eq. 17 is used to determine the fewest grid points required for each method. The results are shown in Fig. 11.

This solution represents a traveling (convecting) wave with a dissipating amplitude. Many methods will convect at the wrong speed (dispersive error) or will excessively dissipate the amplitude (dissipative error).

A key measure of efficiency is how many grid points are required per wavelength to propagate this wave within some predetermined error bound. As k, the wavenumber in Eq. 17 , is increased, the number of grid points must increase to properly simulate the wave.

Currently, Compact schemes are regarded as requiring approximately 6 grid points per wavelength for reasonable solutions. A comparison of the Compact scheme and the UHF schemes with up to 3 spatial derivatives stored on the grid, as shown in the table (Fig. 11(b), demonstrates the Compact scheme is comparable to method $c4o1$ (one solution derivative per grid point). This is expected since the Compact scheme also utilizes 1st derivative information. However, extending Compact schemes to include higher derivatives involves complicated matrices which may be difficult or intractable to solve.

The $c4o3$ method can match the results of the Compact scheme using 16 times fewer grid points per dimension. Specifically, one additional test of the c4o3 method with $k = 8\pi$ and $\Delta x = .2$, the error at $t = 1$ was $2.44291*^{-}5$, which is more accurate than the Compact scheme with considerably fewer grid points per wavelength. Note that the previous comparisons had

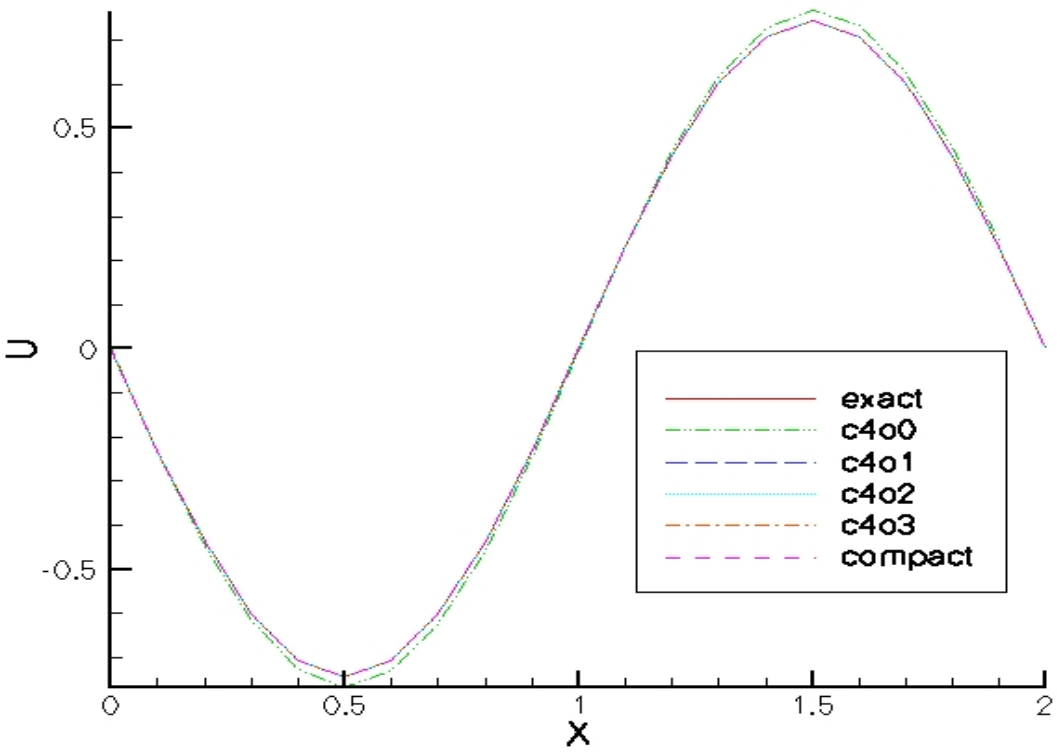

(a) Fidelity Comparison

Method	Spacing	Error
c4o0	.1	$2.54229\,10^{-2}$
c4o0	.2	$4.27563\,10^{-2}$
c4o0	.4	$4.68577\,10^{-2}$
c4o1	.1	$3.11163\,10^{-6}$
c4o1	.2	$2.96551\,10^{-5}$
c4o1	.4	$8.4702\,10^{-4}$
c4o2	.1	$1.0178\,10^{-10}$
c4o2	.2	$3.1935\,10^{-9}$
c4o2	.4	$6.41079\,10^{-8}$
c4o3	.1	$3.44169\,10^{-15}$
c4o3	.2	$2.27818\,10^{-13}$
c4o3	.4	$3.12925\,10^{-11}$
Compact	.1	$1.0993\,10^{-6}$
Compact	.2	$7.10929\,10^{-5}$
Compact	.4	$5.31245\,10^{-3}$

(b) Errors at t=1

Figure 11. Wave Propagation Fidelity

$k = \pi$ and here it was multiplied by eight and we use half as many grid points for a net change of sixteen grid points per wavelength.

Clearly, the UHF schemes are more efficient and can be formulated explicitly for easier parallelization. This implies smoothly transitioning turbulent flows can be more efficiently simulated with UHF techniques.

IX. Conclusion

One-dimensional Navier-Stokes equations are currently utilized for Stirling engine design and optimization with reasonable success. Recent attempts at multi-dimensional simulations have relied upon commercial solvers and this report examined that practice more closely.

This report has shown that the techniques used in commercial codes for simulating Stirling engines are not as capable as more recently developed approaches available in the literature. Moreover, the unique environment of the Stirling engine in which flow is simultaneously turbulent and laminar makes large eddy simulation desirable, while the low Reynold's number, wall bounded flow provides for modest grid requirements and well defined boundary conditions.

Despite the larger stability limit (4 times larger) of Compact schemes for a given grid spacing, the UHF method results in an effective time-step that is 4 times larger than Compact schemes since the grid can be 16 times coarser per dimension. The 6^{th} order Compact schemes performed well with the heat transfer test and apparently would work well in regions of conjugate heat transfer. However, the Compact scheme is not as efficient at predicting turbulent transition compared to UHF methods. The c4o3 method performs similarly to the Compact scheme for steep temperature gradients (conjugate heat transfer) but is up to $16^3 = 4096$ times more efficient when three-dimensional transitional flows need modeled.

It would be desirable to compare c4o4 methods and higher in the future. Future work should examine utilizing UHF methods in a steady-harmonic formulation with Detached Eddy Simulation and more complicated moving grid tests should be performed.

X. Appendix

In what follows are the full equations used to time advance the solutions in this paper and their stability amplification factors. These equations are lengthy, but are provided for completeness and to allow for independent verification.

A. c4o1

The single step c4o1 is given by:

$$
\begin{aligned}
u_i^{n+(1/2)} = \quad & (67)\\
&\left(-\frac{15\mu^3\Delta t^3}{h^6}+\frac{785c\mu^2\Delta t^3}{36h^5}+\frac{45c^2\mu\Delta t^3}{8h^4}-\frac{281c^3\Delta t^3}{1728h^3}+\frac{45\mu^2\Delta t^2}{8h^4}-\frac{281c\mu\Delta t^2}{288h^3}-\frac{27c^2\Delta t^2}{128h^2}-\frac{27\mu\Delta t}{64h^2}+\frac{5c\Delta t}{256h}+\frac{13}{512}\right)u_{i-\frac{3}{2}}\\
&+\left(\frac{15\mu^3\Delta t^3}{h^6}+\frac{345c\mu^2\Delta t^3}{4h^5}-\frac{45c^2\mu\Delta t^3}{8h^4}-\frac{171c^3\Delta t^3}{64h^3}-\frac{45\mu^2\Delta t^2}{8h^4}-\frac{513c\mu\Delta t^2}{32h^3}+\frac{27c^2\Delta t^2}{128h^2}+\frac{27\mu\Delta t}{64h^2}+\frac{405c\Delta t}{256h}+\frac{243}{512}\right)u_{i-\frac{1}{2}}\\
&+\left(\frac{15\mu^3\Delta t^3}{h^6}-\frac{345c\mu^2\Delta t^3}{4h^5}-\frac{45c^2\mu\Delta t^3}{8h^4}+\frac{171c^3\Delta t^3}{64h^3}-\frac{45\mu^2\Delta t^2}{8h^4}+\frac{513c\mu\Delta t^2}{32h^3}+\frac{27c^2\Delta t^2}{128h^2}+\frac{27\mu\Delta t}{64h^2}-\frac{405c\Delta t}{256h}+\frac{243}{512}\right)u_{i+\frac{1}{2}}\\
&+\left(-\frac{15\mu^3\Delta t^3}{h^6}-\frac{785c\mu^2\Delta t^3}{36h^5}+\frac{45c^2\mu\Delta t^3}{8h^4}+\frac{281c^3\Delta t^3}{1728h^3}+\frac{45\mu^2\Delta t^2}{8h^4}+\frac{281c\mu\Delta t^2}{288h^3}-\frac{27c^2\Delta t^2}{128h^2}-\frac{27\mu\Delta t}{64h^2}-\frac{5c\Delta t}{256h}+\frac{13}{512}\right)u_{i+\frac{3}{2}}\\
&+\left(-\frac{5\mu^3\Delta t^3}{h^5}+\frac{55c\mu^2\Delta t^3}{12h^4}+\frac{11c^2\mu\Delta t^3}{8h^3}-\frac{19c^3\Delta t^3}{576h^2}+\frac{11\mu^2\Delta t^2}{8h^3}-\frac{19c\mu\Delta t^2}{96h^2}-\frac{19c^2\Delta t^2}{384h}+\frac{c\Delta t}{256}-\frac{19\mu\Delta t}{192h}+\frac{3h}{512}\right)u_{x_{i-\frac{3}{2}}}\\
&+\left(-\frac{15\mu^3\Delta t^3}{h^5}+\frac{285c\mu^2\Delta t^3}{4h^4}+\frac{57c^2\mu\Delta t^3}{8h^3}-\frac{99c^3\Delta t^3}{64h^2}+\frac{57\mu^2\Delta t^2}{8h^3}-\frac{297c\mu\Delta t^2}{32h^2}-\frac{99c^2\Delta t^2}{128h}+\frac{81c\Delta t}{256}-\frac{99\mu\Delta t}{64h}+\frac{81h}{512}\right)u_{x_{i-\frac{1}{2}}}\\
&+\left(\frac{15\mu^3\Delta t^3}{h^5}+\frac{285c\mu^2\Delta t^3}{4h^4}-\frac{57c^2\mu\Delta t^3}{8h^3}-\frac{99c^3\Delta t^3}{64h^2}-\frac{57\mu^2\Delta t^2}{8h^3}-\frac{297c\mu\Delta t^2}{32h^2}+\frac{99c^2\Delta t^2}{128h}+\frac{81c\Delta t}{256}+\frac{99\mu\Delta t}{64h}-\frac{81h}{512}\right)u_{x_{i+\frac{1}{2}}}+\\
&\left(\frac{5\mu^3\Delta t^3}{h^5}+\frac{55c\mu^2\Delta t^3}{12h^4}-\frac{11c^2\mu\Delta t^3}{8h^3}-\frac{19c^3\Delta t^3}{576h^2}-\frac{11\mu^2\Delta t^2}{8h^3}-\frac{19c\mu\Delta t^2}{96h^2}+\frac{19c^2\Delta t^2}{384h}+\frac{c\Delta t}{256}+\frac{19\mu\Delta t}{192h}-\frac{3h}{512}\right)u_{x_{i+\frac{3}{2}}}
\end{aligned}
$$

$$
\begin{aligned}
(u_x)_i^{n+1} = \quad & (68\\
&\left(\frac{770\mu^3\Delta t^3}{9h^7}+\frac{45c\mu^2\Delta t^3}{h^6}-\frac{785c^2\mu\Delta t^3}{36h^5}-\frac{15c^3\Delta t^3}{8h^4}-\frac{785\mu^2\Delta t^2}{36h^5}-\frac{45c\mu\Delta t^2}{4h^4}+\frac{281c^2\Delta t^2}{576h^3}+\frac{281\mu\Delta t}{288h^3}+\frac{27c\Delta t}{64h^2}-\frac{5}{256h}\right)u_{i-\frac{3}{2}}\\
&+\left(\frac{210\mu^3\Delta t^3}{h^7}-\frac{45c\mu^2\Delta t^3}{h^6}-\frac{345c^2\mu\Delta t^3}{4h^5}+\frac{15c^3\Delta t^3}{8h^4}-\frac{345\mu^2\Delta t^2}{4h^5}+\frac{45c\mu\Delta t^2}{4h^4}+\frac{513c^2\Delta t^2}{64h^3}+\frac{513\mu\Delta t}{32h^3}-\frac{27c\Delta t}{64h^2}-\frac{405}{256h}\right)u_{i-\frac{1}{2}}\\
&+\left(-\frac{210\mu^3\Delta t^3}{h^7}-\frac{45c\mu^2\Delta t^3}{h^6}+\frac{345c^2\mu\Delta t^3}{4h^5}+\frac{15c^3\Delta t^3}{8h^4}+\frac{345\mu^2\Delta t^2}{4h^5}+\frac{45c\mu\Delta t^2}{4h^4}-\frac{513c^2\Delta t^2}{64h^3}-\frac{513\mu\Delta t}{32h^3}-\frac{27c\Delta t}{64h^2}+\frac{405}{256h}\right)u_{i+\frac{1}{2}}\\
&+\left(-\frac{770\mu^3\Delta t^3}{9h^7}+\frac{45c\mu^2\Delta t^3}{h^6}+\frac{785c^2\mu\Delta t^3}{36h^5}-\frac{15c^3\Delta t^3}{8h^4}+\frac{785\mu^2\Delta t^2}{36h^5}-\frac{45c\mu\Delta t^2}{4h^4}-\frac{281c^2\Delta t^2}{576h^3}-\frac{281\mu\Delta t}{288h^3}+\frac{27c\Delta t}{64h^2}+\frac{5}{256h}\right)u_{i+\frac{3}{2}}\\
&+\left(\frac{70\mu^3\Delta t^3}{3h^6}+\frac{15c\mu^2\Delta t^3}{h^5}-\frac{55c^2\mu\Delta t^3}{12h^4}-\frac{11c^3\Delta t^3}{24h^3}-\frac{55\mu^2\Delta t^2}{12h^4}-\frac{11c\mu\Delta t^2}{4h^3}+\frac{19c^2\Delta t^2}{192h^2}+\frac{19\mu\Delta t}{96h^2}+\frac{19c\Delta t}{192h}-\frac{1}{256}\right)u_{x_{i-\frac{3}{2}}}\\
&+\left(\frac{210\mu^3\Delta t^3}{h^6}+\frac{45c\mu^2\Delta t^3}{h^5}-\frac{285c^2\mu\Delta t^3}{4h^4}-\frac{19c^3\Delta t^3}{8h^3}-\frac{285\mu^2\Delta t^2}{4h^4}-\frac{57c\mu\Delta t^2}{4h^3}+\frac{297c^2\Delta t^2}{64h^2}+\frac{297\mu\Delta t}{32h^2}+\frac{99c\Delta t}{64h}-\frac{81}{256}\right)u_{x_{i-\frac{1}{2}}}\\
&+\left(\frac{210\mu^3\Delta t^3}{h^6}-\frac{45c\mu^2\Delta t^3}{h^5}-\frac{285c^2\mu\Delta t^3}{4h^4}+\frac{19c^3\Delta t^3}{8h^3}-\frac{285\mu^2\Delta t^2}{4h^4}+\frac{57c\mu\Delta t^2}{4h^3}+\frac{297c^2\Delta t^2}{64h^2}+\frac{297\mu\Delta t}{32h^2}-\frac{99c\Delta t}{64h}-\frac{81}{256}\right)u_{x_{i+\frac{1}{2}}}\\
&+\left(\frac{70\mu^3\Delta t^3}{3h^6}-\frac{15c\mu^2\Delta t^3}{h^5}-\frac{55c^2\mu\Delta t^3}{12h^4}+\frac{11c^3\Delta t^3}{24h^3}-\frac{55\mu^2\Delta t^2}{12h^4}+\frac{11c\mu\Delta t^2}{4h^3}+\frac{19c^2\Delta t^2}{192h^2}+\frac{19\mu\Delta t}{96h^2}-\frac{19c\Delta t}{192h}-\frac{1}{256}\right)u_{x_{i+\frac{3}{2}}}
\end{aligned}
$$

The c4o1 full step (two staggered half-steps) is:

$$
\begin{aligned}
u_i^{n+1} = & \\
& \left(\frac{770\mu^3\Delta t^3}{9h^7}+\frac{45c\mu^2\Delta t^3}{h^6}-\frac{785c^2\mu\Delta t^3}{36h^5}-\frac{15c^3\Delta t^3}{8h^4}-\frac{785\mu^2\Delta t^2}{36h^5}-\frac{45c\mu\Delta t^2}{4h^4}+\frac{281c^2\Delta t^2}{576h^3}+\frac{281\mu\Delta t}{288h^3}+\frac{27c\Delta t}{64h^2}-\frac{5}{256h}\right)u_{i-\frac{3}{2}} \\
& +\left(\frac{210\mu^3\Delta t^3}{h^7}-\frac{45c\mu^2\Delta t^3}{h^6}-\frac{345c^2\mu\Delta t^3}{4h^5}+\frac{15c^3\Delta t^3}{8h^4}-\frac{345\mu^2\Delta t^2}{4h^5}+\frac{45c\mu\Delta t^2}{4h^4}+\frac{513c^2\Delta t^2}{64h^3}+\frac{513\mu\Delta t}{32h^3}-\frac{27c\Delta t}{64h^2}-\frac{405}{256h}\right)u_{i-\frac{1}{2}} \\
& +\left(-\frac{210\mu^3\Delta t^3}{h^7}-\frac{45c\mu^2\Delta t^3}{h^6}+\frac{345c^2\mu\Delta t^3}{4h^5}+\frac{15c^3\Delta t^3}{8h^4}+\frac{345\mu^2\Delta t^2}{4h^5}+\frac{45c\mu\Delta t^2}{4h^4}-\frac{513c^2\Delta t^2}{64h^3}-\frac{513\mu\Delta t}{32h^3}-\frac{27c\Delta t}{64h^2}+\frac{405}{256h}\right)u_{i+\frac{1}{2}} \\
& +\left(-\frac{770\mu^3\Delta t^3}{9h^7}+\frac{45c\mu^2\Delta t^3}{h^6}+\frac{785c^2\mu\Delta t^3}{36h^5}-\frac{15c^3\Delta t^3}{8h^4}+\frac{785\mu^2\Delta t^2}{36h^5}-\frac{45c\mu\Delta t^2}{4h^4}-\frac{281c^2\Delta t^2}{576h^3}-\frac{281\mu\Delta t}{288h^3}+\frac{27c\Delta t}{64h^2}+\frac{5}{256h}\right)u_{i+\frac{3}{2}} \\
& +\left(\frac{70\mu^3\Delta t^3}{3h^6}+\frac{15c\mu^2\Delta t^3}{h^5}-\frac{55c^2\mu\Delta t^3}{12h^4}-\frac{11c^3\Delta t^3}{24h^3}-\frac{55\mu^2\Delta t^2}{12h^4}-\frac{11c\mu\Delta t^2}{4h^3}+\frac{19c^2\Delta t^2}{192h^2}+\frac{19\mu\Delta t}{96h^2}+\frac{19c\Delta t}{192h}-\frac{1}{256}\right)u_{x_{i-\frac{3}{2}}} \\
& +\left(\frac{210\mu^3\Delta t^3}{h^6}+\frac{45c\mu^2\Delta t^3}{h^5}-\frac{285c^2\mu\Delta t^3}{4h^4}-\frac{19c^3\Delta t^3}{8h^3}-\frac{285\mu^2\Delta t^2}{4h^4}-\frac{57c\mu\Delta t^2}{4h^3}+\frac{297c^2\Delta t^2}{64h^2}+\frac{297\mu\Delta t}{32h^2}+\frac{99c\Delta t}{64h}-\frac{81}{256}\right)u_{x_{i-\frac{1}{2}}} \\
& +\left(\frac{210\mu^3\Delta t^3}{h^6}-\frac{45c\mu^2\Delta t^3}{h^5}-\frac{285c^2\mu\Delta t^3}{4h^4}+\frac{19c^3\Delta t^3}{8h^3}-\frac{285\mu^2\Delta t^2}{4h^4}+\frac{57c\mu\Delta t^2}{4h^3}+\frac{297c^2\Delta t^2}{64h^2}+\frac{297\mu\Delta t}{32h^2}-\frac{99c\Delta t}{64h}-\frac{81}{256}\right)u_{x_{i+\frac{1}{2}}} \\
& +\left(\frac{70\mu^3\Delta t^3}{3h^6}-\frac{15c\mu^2\Delta t^3}{h^5}-\frac{55c^2\mu\Delta t^3}{12h^4}+\frac{11c^3\Delta t^3}{24h^3}-\frac{55\mu^2\Delta t^2}{12h^4}+\frac{11c\mu\Delta t^2}{4h^3}+\frac{19c^2\Delta t^2}{192h^2}+\frac{19\mu\Delta t}{96h^2}-\frac{19c\Delta t}{192h}-\frac{1}{256}\right)u_{x_{i+\frac{3}{2}}}
\end{aligned}
\tag{69}
$$

The real part of c4o1 amplification factor:

$$
\begin{aligned}
\Re(G) \;=\; & (13824^{-1})(32\left(1084v^3-3(8r(1160r-271)+225)v+216\right)\cos(\beta)+ \\
& \left(2248v^3+972(80r-3)v^2-48r(6280r-281)v-\right. \\
& 270v-648r(40r(8r-3)+9)+351)\cos(2\beta)- \\
& 48\beta\left(5760r^3+48(400v-51)r^2-6\left(408v^2+436v-79\right)r+v((237-436v)v+90)\right)\sin(\beta)+ \\
& 81\left(2560r^3+320(46v-3)r^2-24(2v(20v+57)-3)r+\right. \\
& 6v\left(-76v^2+6v+45\right)+28\beta\sin(\beta)+81)- \\
& 3\beta\left(23040r^3+2112(10v-3)r^2-24\left(264v^2+38v-19\right)r-\right. \\
& \left.\left.(2v-3)\left(76v^2-9\right)\right)\sin(2\beta)\right)
\end{aligned}
\tag{70}
$$

The imaginary part of c4o1 amplification factor:

$$
\begin{aligned}
\Im(G) \;=\; & (13824^{-1})(-81\beta\left(2560r^3-1216(10v+1)r^2-8(2v(76v-99)-33)r+\right. \\
& \left.3(2v+1)\left(44v^2-9\right)\right)+ \\
& 6\beta\left(9(82v-39)+4\left(-910v^3-3(1104r-139)v^2+5460r(8r-1)v+\right.\right. \\
& \left.6r(24r(40r-23)+139))\right)\cos(\beta)+ \\
& 3\beta\left(23040r^3+2112(10v-3)r^2-24\left(264v^2+38v-19\right)r-(2v-3)\left(76v^2-9\right)\right)\cos(2\beta) \\
& +2\left(19592v^3-972(80r-3)v^2-6(8r(15560r-2449)+1845)v+\right.
\end{aligned}
\tag{71}
$$

$$27(24r(40r(8r-3)+9)+115))\sin(\beta)$$
$$+\Big(2248v^3+972(80r-3)v^2-48r(6280r-281)v-270v-$$
$$648r(40r(8r-3)+9)+351)\sin(2\beta))$$

B. c4o2

The single step c4o2 (with $r=\mu\frac{\Delta t}{\Delta x^2}$ and $v=c\frac{\Delta t}{\Delta x}$ is:

$$u_i^{n+(1/2)} = \tag{72}$$
$$\left(2835r^5-\tfrac{29575vr^4}{4}-\tfrac{7875r^4}{8}-\tfrac{7875v^2r^3}{4}+\tfrac{113995vr^3}{144}\right)u_{i-\frac{3}{2}}+$$
$$\left(+\tfrac{4425r^3}{32}+\tfrac{113995v^3r^2}{288}+\tfrac{13275v^2r^2}{64}-\tfrac{111115vr^2}{3456}-\tfrac{2025r^2}{256}\right)u_{i-\frac{3}{2}}+$$
$$\left(+\tfrac{4425v^4r}{128}-\tfrac{111115v^3r}{10368}-\tfrac{2025v^2r}{256}+\tfrac{13297vr}{18432}+\tfrac{1215r}{4096}\right)u_{i-\frac{3}{2}}+$$
$$\left(-\tfrac{22223v^5}{41472}-\tfrac{675v^4}{1024}+\tfrac{13297v^3}{110592}+\tfrac{1215v^2}{8192}-\tfrac{155v}{16384}-\tfrac{383}{32768}\right)u_{i-\frac{3}{2}}+$$
$$\left(-2835r^5+\tfrac{250425vr^4}{4}+\tfrac{7875r^4}{8}+\tfrac{7875v^2r^3}{4}-\tfrac{148365vr^3}{16}-\tfrac{4425r^3}{32}\right)u_{i-\frac{1}{2}}+$$
$$\left(-\tfrac{148365v^3r^2}{32}-\tfrac{13275v^2r^2}{64}+\tfrac{98415vr^2}{128}\right)u_{i-\frac{1}{2}}+$$
$$\left(+\tfrac{2025r^2}{256}-\tfrac{4425v^4r}{128}+\tfrac{32805v^3r}{128}+\tfrac{2025v^2r}{256}-\tfrac{80919vr}{2048}-\tfrac{1215r}{4096}\right)u_{i-\frac{1}{2}}+$$
$$\left(+\tfrac{6561v^5}{512}+\tfrac{675v^4}{1024}-\tfrac{26973v^3}{4096}-\tfrac{1215v^2}{8192}+\tfrac{32805v}{16384}+\tfrac{16767}{32768}\right)u_{i-\frac{1}{2}}+$$
$$\left(-2835r^5-\tfrac{250425vr^4}{4}+\tfrac{7875r^4}{8}+\tfrac{7875v^2r^3}{4}+\tfrac{148365vr^3}{16}\right)u_{i+\frac{1}{2}}+$$
$$\left(-\tfrac{4425r^3}{32}+\tfrac{148365v^3r^2}{32}-\tfrac{13275v^2r^2}{64}-\tfrac{98415vr^2}{128}\right)u_{i+\frac{1}{2}}+$$
$$\left(+\tfrac{2025r^2}{256}-\tfrac{4425v^4r}{128}-\tfrac{32805v^3r}{128}+\tfrac{2025v^2r}{256}+\tfrac{80919vr}{2048}-\tfrac{1215r}{4096}\right)u_{i+\frac{1}{2}}+$$
$$\left(-\tfrac{6561v^5}{512}+\tfrac{675v^4}{1024}+\tfrac{26973v^3}{4096}-\tfrac{1215v^2}{8192}-\tfrac{32805v}{16384}+\tfrac{16767}{32768}\right)u_{i+\frac{1}{2}}+$$
$$\left(2835r^5+\tfrac{29575vr^4}{4}-\tfrac{7875r^4}{8}-\tfrac{7875v^2r^3}{4}-\tfrac{113995vr^3}{144}+\tfrac{4425r^3}{32}-\tfrac{113995v^3r^2}{288}\right)u_{i+\frac{3}{2}}+$$
$$\left(+\tfrac{13275v^2r^2}{64}+\tfrac{111115vr^2}{3456}-\tfrac{2025r^2}{256}+\tfrac{4425v^4r}{128}+\tfrac{111115v^3r}{10368}\right)u_{i+\frac{3}{2}}+$$
$$\left(-\tfrac{2025v^2r}{256}-\tfrac{13297vr}{18432}+\tfrac{1215r}{4096}+\tfrac{22223v^5}{41472}-\tfrac{675v^4}{1024}-\tfrac{13297v^3}{110592}\right)u_{i+\frac{3}{2}}+$$
$$\left(+\tfrac{1215v^2}{8192}+\tfrac{155v}{16384}-\tfrac{383}{32768}\right)u_{i+\frac{3}{2}}+$$
$$\left(105h^2r^5-\tfrac{245h^2r^4}{8}-\tfrac{735}{4}h^2vr^4+\tfrac{115h^2r^3}{32}-\tfrac{245}{4}h^2v^2r^3+\tfrac{805}{48}h^2vr^3\right)u_{xx_{i-\frac{3}{2}}}+$$
$$\left(+\tfrac{805}{96}h^2v^3r^2-\tfrac{149h^2r^2}{768}+\tfrac{345}{64}h^2v^2r^2-\tfrac{745h^2vr^2}{1152}\right)u_{xx_{i-\frac{3}{2}}}+$$
$$\left(+\tfrac{115}{128}h^2v^4r-\tfrac{745h^2v^3r}{3456}+\tfrac{29h^2r}{4096}-\tfrac{149}{768}h^2v^2r+\tfrac{29h^2vr}{2048}-\tfrac{149h^2v^5}{13824}\right)u_{xx_{i-\frac{3}{2}}}+$$
$$\left(-\tfrac{149h^2v^4}{9216}+\tfrac{29h^2v^3}{12288}-\tfrac{9h^2}{32768}+\tfrac{29h^2v^2}{8192}-\tfrac{3h^2v}{16384}\right)u_{xx_{i-\frac{3}{2}}}+$$
$$\left(-945h^2r^5+\tfrac{3045h^2r^4}{8}+\tfrac{27405}{4}h^2vr^4-\tfrac{2235h^2r^3}{32}+\tfrac{3045}{4}h^2v^2r^3\right)u_{xx_{i-\frac{1}{2}}}+$$
$$\left(-\tfrac{15645}{16}h^2vr^3-\tfrac{15645}{32}h^2v^3r^2+\tfrac{1863h^2r^2}{256}-\tfrac{6705}{64}h^2v^2r^2\right)u_{xx_{i-\frac{1}{2}}}+$$

$$\left(+\frac{9315}{128}h^2vr^2-\frac{2235}{128}h^2v^4r+\right.$$
$$\left.\frac{3105}{128}h^2v^3r-\frac{1701h^2r}{4096}+\frac{1863}{256}h^2v^2r-\frac{5103h^2vr}{2048}+\frac{621h^2v^5}{512}\right)u_{xx_{i-\frac{1}{2}}}+$$
$$\left(+\frac{621h^2v^4}{1024}-\frac{1701h^2v^3}{4096}+\frac{729h^2}{32768}-\frac{1701h^2v^2}{8192}+\frac{729h^2v}{16384}\right)u_{xx_{i-\frac{1}{2}}}+$$
$$\left(-945h^2r^5+\frac{3045h^2r^4}{8}-\frac{27405}{4}h^2vr^4-\frac{2235h^2r^3}{32}+\frac{3045}{4}h^2v^2r^3+\frac{15645}{16}h^2vr^3+\frac{15645}{32}h^2v^3r^2\right)u_{xx_{i+\frac{1}{2}}}+$$
$$\left(+\frac{1863h^2r^2}{256}-\frac{6705}{64}h^2v^2r^2-\frac{9315}{128}h^2vr^2-\frac{2235}{128}h^2v^4r-\frac{3105}{128}h^2v^3r-\frac{1701h^2r}{4096}+\frac{1863}{256}h^2v^2r+\frac{5103h^2vr}{2048}\right)u_{xx_{i+\frac{1}{2}}}+$$
$$\left(-\frac{621h^2v^5}{512}+\frac{621h^2v^4}{1024}+\frac{1701h^2v^3}{4096}+\frac{729h^2}{32768}-\frac{1701h^2v^2}{8192}-\frac{729h^2v}{16384}\right)u_{xx_{i+\frac{1}{2}}}+$$
$$\left(105h^2r^5-\frac{245h^2r^4}{8}+\frac{735}{4}h^2vr^4+\frac{115h^2r^3}{32}-\frac{245}{4}h^2v^2r^3-\frac{805}{48}h^2vr^3-\right.$$
$$\left.\frac{805}{96}h^2v^3r^2-\frac{149h^2r^2}{768}+\frac{345}{64}h^2v^2r^2+\right)u_{xx_{i+\frac{3}{2}}}+$$
$$\left(\frac{745h^2vr^2}{1152}+\frac{115}{128}h^2v^4r+\frac{745h^2v^3r}{3456}+\frac{29h^2r}{4096}-\frac{149}{768}h^2v^2r-\frac{29h^2vr}{2048}\right)u_{xx_{i+\frac{3}{2}}}+$$
$$\left(+\frac{149h^2v^5}{13824}-\frac{149h^2v^4}{9216}-\frac{29h^2v^3}{12288}-\frac{9h^2}{32768}+\frac{29h^2v^2}{8192}+\frac{3h^2v}{16384}\right)u_{xx_{i+\frac{3}{2}}}+$$
$$\left(1015hr^5-\frac{7945hr^4}{24}-\frac{8925}{4}hvr^4-\frac{7945}{12}hv^2r^3+\frac{4055hr^3}{96}+\frac{10535}{48}hvr^3\right)u_{x_{i-\frac{3}{2}}}+$$

$$\left(+\frac{10535}{96}hv^3r^2+\frac{4055}{64}hv^2r^2-\frac{5401hr^2}{2304}-\frac{9995hvr^2}{1152}+\right)u_{x_{i-\frac{3}{2}}}+$$
$$\left(\frac{4055}{384}hv^4r-\frac{9995hv^3r}{3456}-\frac{5401hv^2r}{2304}+\frac{355hr}{4096}+\frac{1181hvr}{6144}-\frac{1999hv^5}{13824}-\frac{5401hv^4}{27648}\right)u_{x_{i-\frac{3}{2}}}+$$
$$\left(+\frac{1181hv^3}{36864}+\frac{355hv^2}{8192}-\frac{111h}{32768}-\frac{41hv}{16384}\right)u_{x_{i-\frac{3}{2}}}+$$
$$\left(945hr^5-\frac{2205hr^4}{8}+\frac{89775}{4}hvr^4-\frac{2205}{4}hv^2r^3+\frac{555hr^3}{32}-\frac{58695}{16}hvr^3\right)u_{x_{i-\frac{1}{2}}}+$$
$$\left(-\frac{58695}{32}hv^3r^2+\frac{1665}{64}hv^2r^2+\frac{1377hr^2}{256}+\frac{44145}{128}hvr^2+\frac{555}{128}hv^4r\right)u_{x_{i-\frac{1}{2}}}+$$
$$\left(\frac{14715}{128}hv^3r+\frac{1377}{256}hv^2r-\frac{6075hr}{4096}-\frac{38637hvr}{2048}+\frac{2943hv^5}{512}+\right.$$
$$\left.\frac{459hv^4}{1024}-\frac{12879hv^3}{4096}-\frac{6075hv^2}{8192}+\frac{5103h}{32768}+\frac{8019hv}{16384}\right)u_{x_{i-\frac{1}{2}}}+$$
$$\left(-945hr^5+\frac{2205hr^4}{8}+\frac{89775}{4}hvr^4+\frac{2205}{4}hv^2r^3-\frac{555hr^3}{32}-\frac{58695}{16}hvr^3-\frac{58695}{32}hv^3r^2-\frac{1665}{64}hv^2r^2\right)u_{x_{i+\frac{1}{2}}}+$$
$$\left(-\frac{1377hr^2}{256}+\frac{44145}{128}hvr^2-\frac{555}{128}hv^4r\right)u_{x_{i+\frac{1}{2}}}+$$
$$\left(\frac{14715}{128}hv^3r-\frac{1377}{256}hv^2r+\frac{6075hr}{4096}-\frac{38637hvr}{2048}+\frac{2943hv^5}{512}\right)u_{x_{i+\frac{1}{2}}}+$$
$$\left(-\frac{459hv^4}{1024}-\frac{12879hv^3}{4096}+\frac{6075hv^2}{8192}-\frac{5103h}{32768}+\frac{8019hv}{16384}\right)u_{x_{i+\frac{1}{2}}}+$$
$$\left(-1015hr^5+\frac{7945hr^4}{24}-\frac{8925}{4}hvr^4+\frac{7945}{12}hv^2r^3-\frac{4055hr^3}{96}+\frac{10535}{48}hvr^3+\frac{10535}{96}hv^3r^2-\frac{4055}{64}hv^2r^2+\right)u_{x_{i+\frac{3}{2}}}$$
$$\left(\frac{5401hr^2}{2304}-\frac{9995hvr^2}{1152}-\frac{4055}{384}hv^4r-\frac{9995hv^3r}{3456}+\frac{5401hv^2r}{2304}-\frac{355hr}{4096}+\frac{1181hvr}{6144}\right)u_{x_{i+\frac{3}{2}}}$$
$$\left(-\frac{1999hv^5}{13824}+\frac{5401hv^4}{27648}+\frac{1181hv^3}{36864}-\frac{355hv^2}{8192}+\frac{111h}{32768}-\frac{41hv}{16384}\right)u_{x_{i+\frac{3}{2}}}$$

The double step from u_i^n to u_i^{n+1} can be immediately derived by using two single steps above. The equations are ommitted due to length.

1. c4o2 Amplification

The equations for the amplification factor of this method are sufficiently large that their full form is not shown. Please see Ref.[41] for the complete form.

XI. Acknowledgements

The work described in this paper was performed for the Science Mission Directorate (SMD) and the Radioisotope Power System (RPS) Program, which provided funding for these projects. The opinions expressed in this paper are those of the authors.

References

[1]Beale, W.T.:"Free Piston Stirling Engines - Some Model Tests and Simulations", [Preliminary investigation of free-piston Stirling engines.], SAE International Automtive Engineering Conference, Jan. 1969

[2]Thieme, L.G.; Schreiber, J.G. : "NASA GRC Stirling Technology Development Overview", NASA/TM-2003-212454, Aug. 2003

[3]Cengel, Y.A.; Boles, M.A. : "Thermodynamics: An Engineering Approach", McGraw-Hill, 1989

[4]Tew, R.C., Thieme, L.G., Dudenhoefer, J.E. : "Recent Stirling Engine Loss-Understanding Results", 25th IECEC, NASA TM 103122, 1990

[5]Hirata, K., Kagawa, N., Takeuchi, M., Yamashita, I., Isshiki, N., Hamaguchi, K. : "Test Results of Applicative 100 W Stirling Engine", 96204.

[6]Ibrahim, M.B., Tew, R.C., Zhang, Z., Gedeon, D. Simon, T. : "CFD Modeling of Free-Piston Stirling Engines", NASA/TM-2001-211132, IECEC2001-CT-38, Sept. 2001.

[7]Dyson, R.W., "Technique For Very High Order Nonlinear Simulation and Validation", J. Comp. Acoustics, Vol. 10, No. 2, pp. 211-229, 2002.

[8]Carpenter, M.H., Nordstrom, J., Gottlieb, D. "A Stable and Conservative Interface Treatment of Arbitrary Spatial Accuracy", Institute for Computer Applications in Science and Engineering (ICASE) Report No. 98-12, 1998.

[9]Carpeneter, M.H., Casper, J.H. "The Accuracy of Shock Capturing in Two Spatial Dimensions", AIAA 97-2107, July 1997.

[10]Tew, R.C., Ibrahim, M.B. : "Two-dimensional Compressible Non-Acoustic Modeling of Stirling Machine-Type Components", J. of Prop. and Power, Vol. 19, No. 5, Sept.-Oct. 2003

[11]Thieme, L.G., Schreiber, J.G., Mason, L.S. : "Stirling Technology Development at NASA GRC", NASA/TM-2001-211315/REV1, Jan. 2002

[12]Schreiber, J. : "Tutorial on Free-Piston Stirling Power Conversion Technology (How Does it Work?), Space Technology and Applications International Forum, Feb. 2001

[13]Furlong, R., Shaltens, R. : "Technology Assessment of DOE's 55-We Stirling Technology Demonstrator Convertor (TDC)", NASA/TM-2000-210509, Oct. 2000

[14]Stanescu, D., Habashi, W.G., "2N-Storage Low Dissipation and Dispersion Runge-Kutta Schemes for Computational Acoustics", *Journal of Computational Physics, Vol 143, no. 2, 1998, pp. 674.*

[15] *Goodrich, J.W., "A Comparison of Numerical Methods for Computational Aeroacoustics", AIAA 99-1943, May 1999.*

[16] *Goodrich, J.W., "Application of a New High Order Finite Difference Scheme to Acoustic Propagation With the Linearized Euler Equation," NASA/TM-1993-106454, June 1993.*

[17] *Goodrich, J.W. "Accurate Finite Difference Algorithms for Computational Aeroacoustics",* Computational Fluid Dynamics Review 1998, edited by M.M Hafez and K. Oshima, World Scientific, Singapore, 1998.

[18] Garabedian, P.R., "The Method of Power Series:The Cauchy-Kowalewski Theorem," *Partial Differential Equations, 2nd ed., Chelsea, New York, 1986, pp. 6-16.*

[19] *Goodrich, J.W., "An Approach to the Development of Numerical Algorithms for First Order Linear Hyperbolic Systems in Multiple Space Dimensions:The Constant Coefficient Case," NASA/TM-1995-106928, September 1995.*

[20] *Dyson, R.W., "Demonstration of Ultra HI-FI Methods", Int. J. of Computational Fluid Dynamics", accepted for publication.*

[21] *Dyson, R.W., Goodrich, J.W. "A Very High Order, Adaptable MESA Implementation for Aeroacoustic Computations", NASA/TM-2000-209944, April 2000.*

[22] *Hoffman, K.A., Chiang, S.T., "Computational Fluid Dynamics For Engineers – Volume I and II", Engineering Education System, Wichita, Kansas, 1993*

[23] *Anderson, D.; Tannehill, J.C. ; Pletcher, R.H. : "Computational Fluid Mechanics and Heat Transfer", McGraw-Hill, 1984.*

[24] *Chung, T.J. : "Computational Fluid Dynamics", Cambridge University Press, 2002, pp. 394.*

[25] *Sun, Y. ; Wang, Z.J. : "High-Order Spectral Volume Method for the Navier-Stokes Equations on Unstructured Grids", AIAA-2004-2133, 2004*

[26] *Benton, E.R. ; Platzman, G.W. : "A Table of Solutions of the One-dimensional Burgers Equation, Q. Appl. Math., vol. 30, pp. 195-212, 1972.*

[27] *Lele, S.K.: "Compact finite difference schemes with spectral-like resolution", J. Comp. Phys., 183, 16-42., 1992*

[28] *Patankar, S.V. and Spalding, D.B., "A Calculation procedure for heat, mass and momentum transfer in three-dimensional parabolic flows.", Int. J. Heat Mass Transfer, 15, 1787-1806.*

[29] *Issa, R. I., "Solution of the implicitly discretized fluid flow equations by operator splitting.", 62, 40-65 of compressible and incompressible recirculating flows by a non-iterative scheme", J. Comp. Phys., 62, 66-82.*

[30] *Issa, R. I., Gosman, A.D., and Watkins, A.P., "The computation of compressible and incompressible recirculating flows by a non-iterative scheme", J. Comp. Phys., 62, 66-82.*

[31] *Anderson, J.D., "Computational Fluid Dynamics: the Basics with Applications", McGraw-Hill, 1995*

[32] *Gedeon, D. : "GLIMPS Version 4: User's Manual", Gedeon Associates, July 1992.*

[33] *Huang, S.C. : "HFAST - A harmonic analysis program for Stirling cycles", AIAA International Energy Conversion Engineering Conference, Vol. 5, p. 47-52, 1992*

[34] *Fletcher, C.A.J. : "Computational Techniques for Fluid Dynamics - Volume I", Springer-Verlag, 1988.*

[35] *Simon, T.W. and J.R. Seume : "A Survey of Oscillating Flow in Stirling Engine Heat Exchangers", NASA-CR-182108, Mar. 1988.*

[36] *Ahn, K.H., Ibrahim, M.B., "Turbulent Oscillating Flow in Circular Pipes", Int. J. of Heat and Fluid Flow, 13(4):340-346, Dec. 1992*

[37] *Oseid, K.L. : "Numerical Prediction of Turbulent Oscillating Flow and Heat Transfer in Pipes with Various End Geometries", NASA CR 198416, Oct. 1995*

[38] *Walther, C., Kuhl, H.D., Schulz, S., "Numerical Investigations on the Heat Transfer in Turbulent Oscillating Pipe Flow", Heat and Mass Transfer, 36(2): 135-141, Apr. 2000.*

[39] *Wilcox, D.C., "Turbulence Modeling for CFD", DCW Industries, 2000.*

[40] *West, C.D. : "Principles and Applications of Stirling Engines", Van Nostrand Reinhold Company, New York, 1986.*

[41] *Dyson, R.W., Wilson, S. D., Tew, R.C., Demko, R. "Stirling Analysis Comparison of Commercial VS. High-Order Methods", NASA-TM-2005-213976, October 2005*